

Sizing of chillers with thermal and battery storage for enhanced integration with on-site PV

Al-Aali, I.^{1*}, Narayanaswamy, A.^{1*}, Modi, V.^{1*}

¹Mechanical Engineering Department, Columbia University, New York City, United States

Abstract

Space-cooling is dominating building energy use in warm regions. Integrating on-site PV generation with cooling systems is a potential building-scale decarbonization solution. However, designing the system to ensure cost-effectiveness and reliability is challenging since it requires solving a highly non-linear design and dispatch problem. This paper proposes a solution strategy to the design problem of an integrated multi-chillers system with PV, and ice thermal and battery storage to reduce annual system costs. The proposed strategy adopts a bi-level optimization approach eliminating the need for simplistic models. The upper level employs particle swarm optimization to determine storage and chillers' capacities and types, while the lower level solves the dispatch problem using mixed-integer linear programming. To validate the proposed strategy and decarbonization solution, the model was applied to a generic residential building in Qatar and was exposed to a varying range of carbon pricing. The results highlight the potential for deep decarbonization in regions with abundant solar resources and high cooling needs. In Qatar, the model suggests a moderate carbon pricing range of \$75-125/ton of CO₂ for deep decarbonization. The developed model demanded reasonable computational resources with an execution time of less than 1 hour and exhibited stability with consistent convergence.

Highlights:

- Design of multi-chiller system with ice and battery storage for integration with PV
- Optimization strategy to decide chillers' quantities, capacities, and types
- Piecewise linear chillers and ice storage models
- Distributed scale decarbonization solution for cooling-intensive regions

Keywords: Ice storage; Thermal storage; Chilled water system; Battery energy storage system; PV generation; Load shifting; Peak shaving; Equipment capacity sizing

*Corresponding authors. Department of Mechanical Engineering, Columbia University, New York 10027

¹ Email Addresses: iaa2111@columbia.edu (Al-Aali, I.), arvind.narayanaswamy@columbia.edu (Narayanaswamy, A.), modi@columbia.edu (Modi, V.)

Nomenclature

Parameters

Symbol	Meaning
$a_{f,m}^S$	Storage heat rate curve slope for piecewise linear segment f and mode of operation m , [kW _{th}]
$a_{x,j,m,e}^{chl}$	Chiller power curve slope for piecewise linear segment f and mode of operation m , [kW _{th}]
$b_{f,m}^S$	Storage heat rate curve y-intercept for piecewise linear segment f and mode of operation m , [kW _{th}]
$b_{x,j,m,e}^{chl}$	Chiller power curve y-intercept for piecewise linear segment f and mode of operation m , [kW _{th}]
c^{BESS}	Capital cost of installed battery capacity, [\$/kWh]
$c^{PV,C}$	Capital cost of installed fixed-tilt PV capacity, [\$/kW _{p,dc}]
c^{ITES}	Capital cost of installed ice storage capacity, [\$/kWh _{th}]
c_x^{chl}	Capital cost of installed chiller capacity with compressor technology x , [\$/kW _{th}]
$c^{P,FS}$	Capital cost of installed fixed speed pumps, [\$/kW]
$c^{P,VSD}$	Capital cost of installed variable speed pump, [\$/kW]
c^{twr}	Capital cost of installed cooling tower, [\$/kW _{th}]
$c_s^{PV,O}$	Operating cost of installed fixed-tilt PV capacity, [\$/kW _{p,dc} /yr.]
c^e	Cost of electricity from the power grid, [\$/kWh]
c^P	Demand charge, [\$/kW _p]
C^{Calmac}	Usable capacity of modular ice storage tank (83-TR-hr nominal), [kWh _{th}]
$COP_{x,j}$	Nominal coefficient of performance of chiller j with compressor technology x , dimensionless
$COP_{x,j}^{adj}$	Adjusted coefficient of performance of chiller j with compressor technology x , dimensionless
\mathcal{L}^{Elec}	Hourly electric load, [kW]
\dot{m}^{iw}	Maximum available flowrate for ice storage, [kg/s]
$\dot{m}^{iw,max}$	Maximum allowable flowrate for ice storage, [kg/s]
$\dot{m}_{x,j}^{sw}$	Design supply water flowrate of chiller j with compressor technology x , [kg/s]
M	Arbitrarily large number (Big M)
N^{chl}	Number of chillers, dimensionless
N^{ITES}	Number of modular ice tanks, dimensionless
N_p^{days}	Number of days represented by scenario p , dimensionless
N_p^{mos}	Number of months represented by scenario p , dimensionless
$p_{cf,des}$	Coils fan power use at design conditions, [kW]
$p_{x,j}^{cp,des}$	Power use of condenser pump from chiller j with compressor technology x , [kW]
$p_{x,j}^{pp,des}$	Power use of primary pump from chiller j with compressor technology x , [kW]
$p_{sp,des}$	Variable speed pumps power use at design conditions, [kW]
$p_{twr,des}$	Cooling tower power use at design conditions, [kW]
$PLR_{x,m,e}^{ll}$	Lower part load ratio limit of chiller with compressor technology x in segment e under operating mode m , dimensionless

$PLR_{x,m,e}^{ul}$	Upper part load ratio limit of chiller with compressor technology x in segment e under operating mode m , dimensionless
$Q_{p,t}^D$	Building cooling demand at time t and scenario p , [kW _{th}]
$\overline{Q^{chl,des}}$	Upper limit for decided chiller nominal capacity, [kW _{th}]
$\underline{Q^{chl,des}}$	Lower limit for decided chiller nominal capacity, [kW _{th}]
\dot{Q}_x^{ref}	Reference nominal capacity of chiller with compressor technology x , [kW _{th}]
$T_{p,t}^{csw}$	Entering condenser water temperature at time t and scenario p , [°C]
$T_{p,t}^{wb}$	Ambient wet-bulb temperature at time t and scenario p , [°C]
T^{sw}	Supply water temperature, [°C]
$T_{rw,des}$	Design return water temperature, [°C]
yr	Service life of PV, ice chillers, and ice storage, [yrs.]
yr_b	Battery service life, [yrs.]
$\eta^{BESS,chs}$	Battery charge efficiency, dimensionless
$\eta^{BESS,dis}$	Battery discharge efficiency, dimensionless
$\eta^{BESS,sdis}$	Battery self-discharge efficiency, dimensionless
η^I	Inverter efficiency, dimensionless
$\Delta T^{app,des}$	Design cooling tower approach temperature, [°C]
$\Delta T^{cond,ref}$	Reference chillers condenser temperature differential, [°C]
$\Delta T^{evap,ref}$	Reference chillers evaporator temperature differential, [°C]

Decision variables

Symbol Meaning

$B_{p,t}^{chs}$	Battery charging rate at time t and scenario p , [kW]
$B_{p,t}^{dis}$	Battery discharging rate at time t and scenario p , [kW]
$B_{p,t}^S$	Stored electric energy at time t and scenario p , [kWh]
$B_{p,t,x,j,m,e}^{chl}$	Binary variable to toggle on chiller power curve piecewise linear segment e in operation mode m for chiller j with compressor technology x at time t and scenario p , binary
$B_{p,t}^{ice}$	Binary variable to activate ice-making mode at time t and scenario p , binary
$B_{p,t,m,f}^{ITES}$	Binary variable to toggle on ice storage heat rate curve piecewise linear segment f in operation mode m at time t and scenario p , binary
C^{BESS}	Installed BESS capacity, [kWh]
C^{PV}	Installed on-site fixed-tilt PV capacity, [kW _{p,dc}]
C^p	Installed cumulative chiller pumps capacity, [kW]
C^{sp}	Installed variable speed pumps capacity, [kW]
C^{twr}	Installed cooling tower capacity, [kW _{th}]
G^P	Peak gas generation demand, [kW]
$G_{p,t}$	Power delivered by the electricity grid at time t and scenario p , [kW]
N^{ITES}	Number of modular ice storage tanks, $N^{ITES} \in \mathbb{R}$
$S_{p,t}^{chs}$	Ice storage charge rate at time t and scenario p , [kW _{th}]
$S_{p,t}^{dis}$	Ice storage discharge rate at time t and scenario p , [kW _{th}]
$S_{p,t}^S$	Stored thermal energy at time t and scenario p , [kWh _{th}]

$ON_{p,t,x,j}^{chl}$	Power switch for chiller j with compressor technology x at time t and scenario p , binary
$PV_{p,t}^{curt}$	Curtailed PV generation at time t and scenario p , [kW]
$P_{p,t}^{aux}$	Auxiliary equipment power use at time t and scenario p , [kW]
$P_{p,t}^{dist}$	Distribution equipment power use at time t and scenario p , [kW]
$P_{p,t}^p$	Pumps power use at time t and scenario p , [kW]
$P_{p,t}^{twr}$	Cooling tower power use at time t and scenario p , [kW]
$\dot{Q}_{p,t,x,j}^{chl}$	Load for chiller j with compressor technology x at time t and scenario p , [kW _{th}]
$\dot{Q}_{p,t}^{chl,tot}$	Total chillers load at time t and scenario p , [kW _{th}]
$Q_{x,j}^{chl,des}$	Decided nominal capacity of chiller j with compressor technology x , [kW _{th}]
$\Delta T^{cond,des}$	Design chillers condenser water temperature differential, [°C]
$\Delta T^{evap,des}$	Design chillers evaporator water temperature differential, [°C]

Index sets

Symbol Meaning

e	Chiller piecewise linear segment index set $\{1, 2\}$ denoted by \mathcal{E}
f	Storage piecewise linear segment index set $\{1, 2, 3, 4\}$ denoted by \mathcal{F}
j	Chiller index set $\{1, 2, 3, \dots\}$ such that $j \in \mathbb{N}$
m	Operation mode index set $\{1, 2\}$ denoted by \mathcal{M}
p	Scenario index set $\{1, 2, 3, 4, 5\}$ denoted by \mathcal{P}
t	Time step index set $\{1, 2, 3, 4, \dots, 24\}$ denoted by \mathcal{T}
x	Chiller compressor technology index set $\{1, 2, 3\}$ denoted by \mathcal{X}

1. Introduction

Threatened by climate catastrophe due to anthropogenic carbon emissions, the world needs to adopt more sustainable approaches to meet increasing energy demand. World energy use is responsible for two-thirds of yearly anthropogenic carbon emissions [1], which can be classified into three end-use sectors: transportation, industrial, and buildings. Worldwide, building energy use accounts for 30% of total energy end-use and 55% of electricity use [2] and is dominated by space-cooling and heating and domestic hot water needs [3,4]. In cooling-intensive regions, year-round space-cooling needs are responsible for most electricity use [5].

Warmer arid regions with high cooling needs are deemed to be well suited for exploiting solar PV (photovoltaics) in multiple analyses [6–9] since they have abundant and predictable solar irradiation synergistic with electricity demand. With a hot summer and milder winter, the cooling load is highly seasonal. This seasonality naturally leads to a large sum of idle cooling capacity in the shoulder season that could be utilized to store thermal energy for nighttime cooling needs. Integrating PV generation with energy storage technologies is a potential building-scale decarbonization solution. However, it remains a challenge to optimize the system design to ensure cost-effectiveness and reliability since it requires solving a highly non-linear design and dispatch problem. This paper examines the building-scale design problem of an integrated multi-chillers system with I-TES (ice thermal energy storage), BESS (battery energy storage system), and on-site PV generation for costs and emissions reduction. I-TES stores thermal energy in the form of ice that can be used later for cooling.

In the literature, the design problem of building-scale PV with BESS and thermal energy storage falls under the smart building energy management systems problem, which is broadly investigated with varying degrees of complexity. Many studies recognize the potential of using I-TES for cost reduction but find BESS cost-prohibitive. Deetjen et al. [10] developed a mixed-integer linear programming model for optimal dispatch and sizing of a residential central utility plant with a rooftop PV generation, shared I-TES, and BESS. The model accounts for chillers' performance degradation from ambient conditions and in ice-making mode. Although the study finds cost reduction potential from the examined system, BESS was still determined to be economically unfavorable. Baraa et al. [11] analyzed micro-grid design with BESS and I-TES applied to a commercial building in the UAE using a heuristically developed optimization strategy. The I-TES model was extracted from EnergyPlus, with linearized charge/discharge limits with respect to the storage state of charge. Baraa concludes that I-TES further reduces the cost compared to BESS alone. Zhu et al. [12] proposed a bi-level optimization strategy to optimize electric and thermal energy storage capacity in buildings with a chilled water system. The upper level decides the capacities and the lower level solves the dispatch problem and returns the operation cost. The optimization strategy utilizes the genetic algorithm for the upper level and mixed-integer linear programming with a piecewise linearized chiller model for the lower level. The study suggests that energy storage can significantly reduce cost and increase renewable penetration in the grid from

load shifting. Xu et al. [13] developed a two-stage stochastic linear model for capacity and dispatch optimization of building-scale PV combined with BESS, I-TES, and heat storage. They consider a simple linear I-TES model with a single chiller. Xu finds TES to be economically favorable whereas BESS is not always feasible due to its higher cost and short life span.

A common solution strategy in the literature is to discriminately simplify the models and solve them using meta-heuristic algorithms. While the optimization strategies are useful for broad energy analysis, they tend to fall short at the systems design level. This paper proposes an improved strategy that negates the need for simplistic models. The proposed strategy better accounts for the complex operation and performance of chillers and I-TES than previously done in the literature, which includes deciding multi-chiller capacities and types while accounting for their part-load performance and the impact of intra-annual ambient temperature variations. The developed strategy splits the problem into a bi-level optimization formulation. The upper level decides the storage and chillers' capacities and the lower level solves the dispatch problem. Physics-based models of the main power-consuming devices were used as a foundation to build piecewise linearized component models. To evaluate the developed strategy and the proposed decarbonization solution, the model was applied to a generic residential building in Qatar and exposed to a range of carbon pricing to help promote the adoption of sustainable energy resources. Carbon pricing is a policy tool that adds a cost to electricity generation per ton of CO₂ emitted.

The paper is structured as follows: Section 2 describes the methodology. First, the optimization strategy is described, followed by the developed components models and overall problem formulation. Next, cooling and electric loads are simulated for a generic residential building in Qatar that is used for model evaluation. Section 3 presents and discusses the results. The paper is summarized and concluded in Section 4.

2. Methodology

The overall framework utilizes on-site PV generation to meet daytime electricity and cooling needs. Excess generation can be stored in I-TES and BESS to supplement nighttime electricity and cooling needs; unutilized excess generation is curtailed. Due to the overlap of peak cooling hours with the solar insolation, chillers' cumulative cooling capacity can exceed the building's peak cooling load to allow for ice-making during the day. Figure 1 shows a simplified schematic of the design problem. The WC CWS is in the common primary-secondary configuration [14]. A large residential building is examined for the optimization problem. The examination of a large building serves two purposes, (i) large buildings tend to utilize WC CWS, which enables exploring the more complex version of the problem due to additional equipment such as cooling towers; (ii) large systems achieve higher returns and emissions reduction and are a primary target for decarbonization.

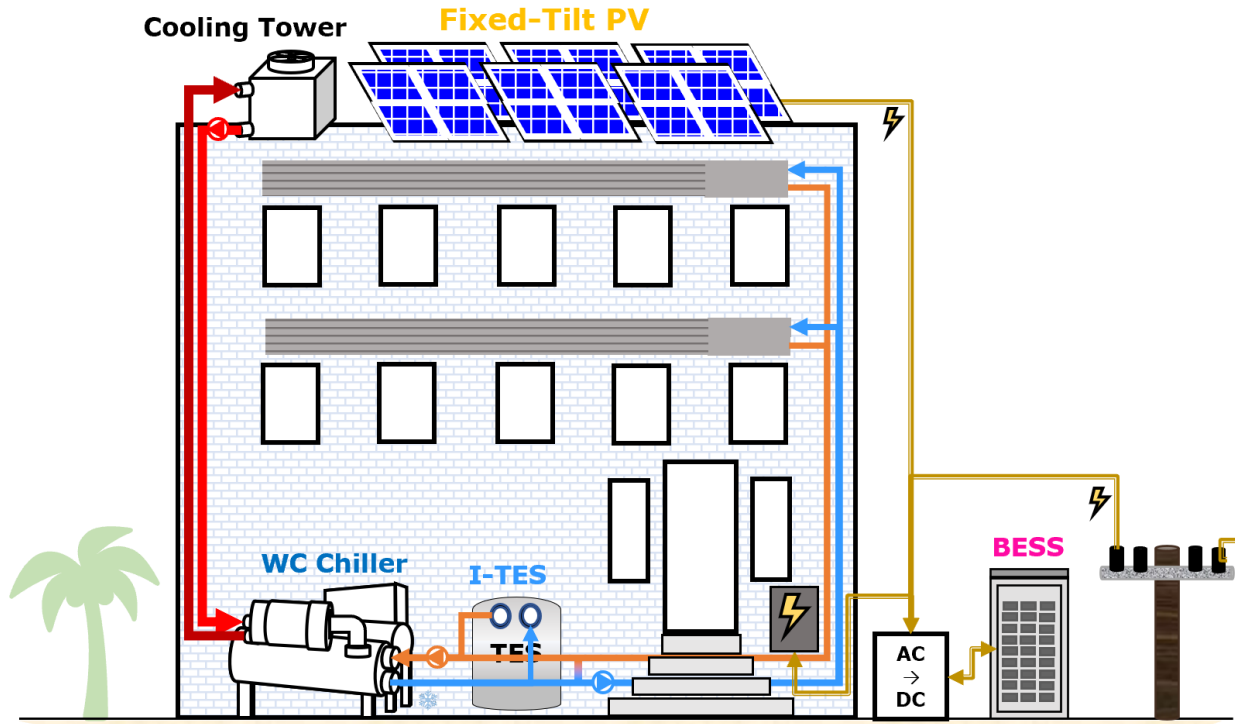


Figure 1: A schematic of an integrated WC CWS with I-TES, BESS, and on-site PV generation.

2.1 Optimization strategy

Optimal capacity sizing of system components entails estimating their energy use, which requires solving the complex scheduling and dispatch problem. The complexity stems from the non-linear interaction of multiple decision variables at each time step [15]. For instance, water-cooled chiller power use is a function of 4 parameters at each time step: supply temperature setpoint, entering condenser water temperature, cooling load, and the power switch, in addition to the chiller capacity decision variable. Likewise, I-TES charge and discharge rates are a function of 3 parameters at each time step: the inlet temperature and flowrate, and the state of charge, in addition to the storage capacity decision variable.

A problem with this level of complexity is too computationally demanding to be solved using traditional gradient-based optimization strategies or more tolerant meta-heuristics optimization algorithms. The approach is to decompose the problem into a bi-level formulation that allows for the decoupling of the capacity sizing problem from the scheduling and dispatch problem. The scheduling and dispatch problem can then be simplified in a mixed-integer linear program with piecewise linearized performance curves that can be promptly solved whilst having hundreds of variables. Meta-heuristic algorithms are suitable for the upper level because they are broad and can work with non-convex and non-linear models and are widely used in air conditioning problems. They work by propping the search space using a population of potential solutions.

Examples are particle swarm optimization and genetic algorithm. Particle swarm optimization is more suitable for the examined problem because it is more computationally efficient.

A flowchart of the developed bi-objective optimization strategy is shown in Figure 2. The upper level minimizes annual system expenditures and decides the installed components' capacities using particle swarm optimization. Piecewise linearization is then applied to the components' performance curves to build a mixed-integer linear program in the lower level that is solved to estimate annual system electricity consumption. The estimated electricity charges are returned to the upper-level optimizer to update the capacities for the next iteration.

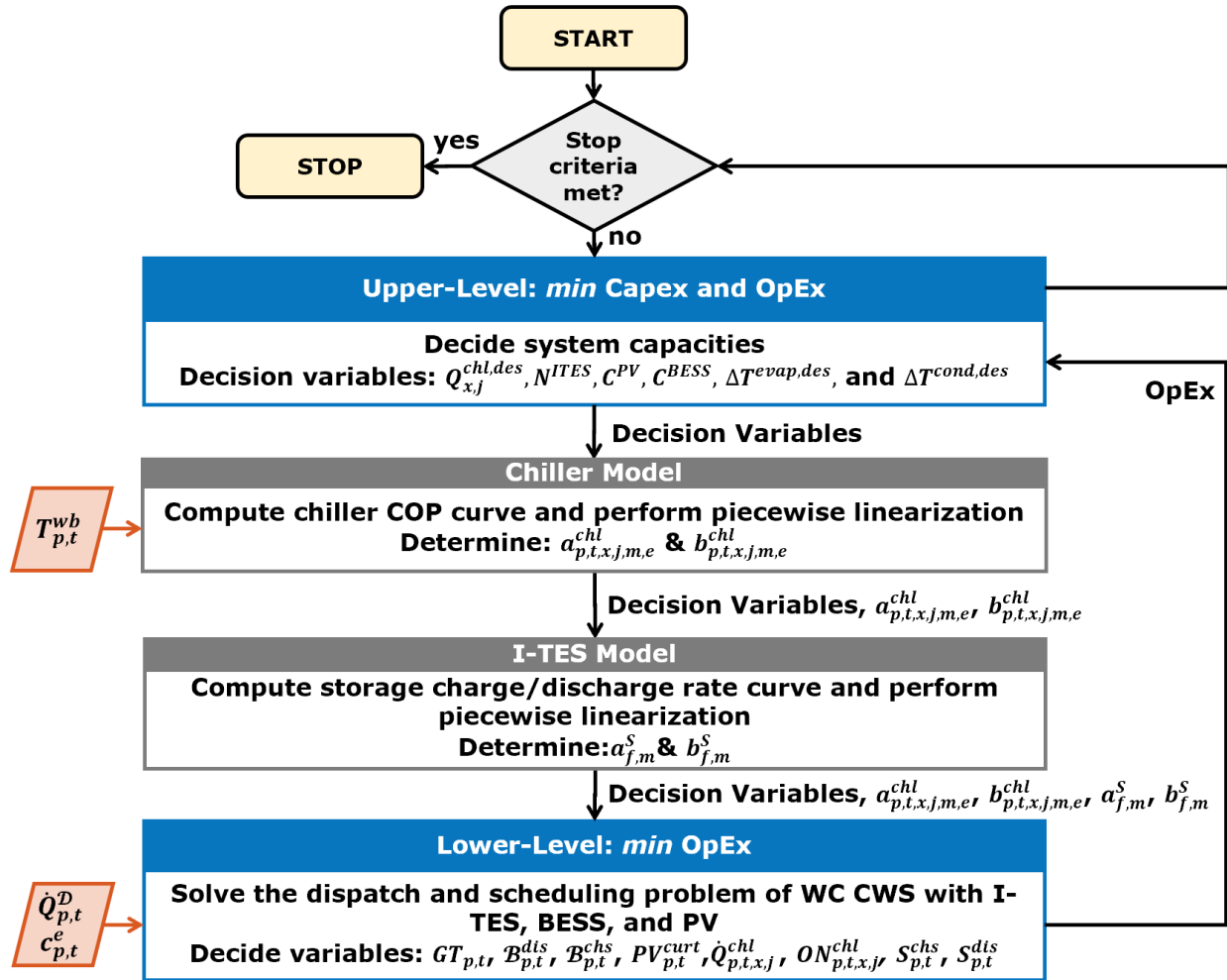


Figure 2: Bi-level optimization formulation. The upper level minimizes annual system costs and decides the installed capacities and the lower level solves the equipment scheduling and dispatch problem in a mixed-integer linear programming formulation and returns system electricity use.

2.2 Components modeling

Water-cooled chilled water systems contain various components including chillers, pumps, valves, cooling towers, and cooling and dehumidification coils. A common well-established chilled water system configuration is primary-secondary flow, shown in Figure 3. This configuration decouples the secondary loop from the primary loop. The chillers operate with their respective fixed-speed pumps to maintain design flow. In conjunction with two-way valves, variable-speed drive (VSD) pumps modulate the water supply to the coils to satisfy the building's load. Surplus water returns through the decoupler blending with the coils' return water. The I-TES is located downstream of the chillers, allowing chillers to receive warmer building return water and operate more efficiently. A water-glycol mixture is used in the evaporator to prevent freezing when operating near or at sub-freezing temperatures needed to store ice, which depresses the thermal capacity of the mixture by about 10% relative to pure water.

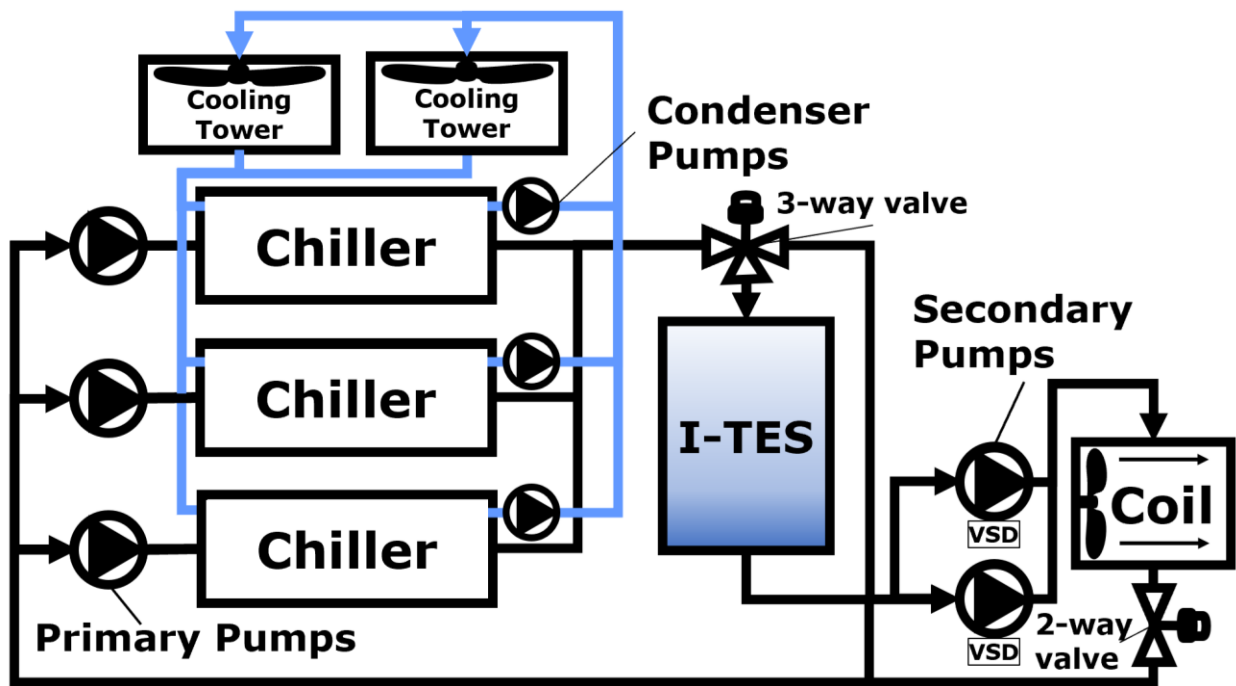


Figure 3: Chilled water system in a primary-secondary flow configuration.

Piecewise linear models are developed for the major power-consuming devices, which include (i) chillers, (ii) water pumps, and (iii) I-TES. Electricity consumption for auxiliary devices such as cooling towers and cooling coils with complex performance characteristics that only minorly contribute to power consumption are crudely estimated.

Chillers

Chillers are the main energy-consuming device in chilled water systems. The efficiency of a chiller measured by the COP is a function of its loading, and evaporator and condenser temperatures. The COP can be modeled as a function of two parameters: loading and the on/off switch suitable for

mixed integer linear programming when the supply and entering condenser temperatures are pre-determined, which is often done in the literature in optimal chiller loading problems [16–18]. The entering condenser temperature is related to the wet-bulb temperature; a reasonable approximation is to use the design tower approach temperature to infer their relationship, as described below:

$$T_{p,t}^{csw} = T_{p,t}^{wb} + \Delta T^{app,des} \quad (1)$$

where subscripts p is the scenario index set $\{1, 2, 3, 4, 5\}$ denoted by \mathcal{P} that corresponds to selected representative days of the year and t is the time step index set $\{1, 2, 3, \dots, 24\}$ denoted by \mathcal{T} and corresponds to hours of the day, and $\Delta T^{app,des}$ is the design tower approach temperature, typically in the order of 3°C. The refrigerant condensing temperature is dictated by the entering condenser water temperature and the decided temperature differential, as described by the following equation:

$$T_{p,t}^{crw} = T_{p,t}^{csw} + \Delta T^{cond,des} \quad (2)$$

where $\Delta T^{cond,des}$ is the design condenser water temperature differential and is a decision variable. The decided temperature differential is inversely related to the flowrate and correlates cubically with pump energy use, per the affinity laws.

Likewise, the supply setpoint temperature is determined based on the operating mode of the chillers: ice-making or refrigeration. In ice-making mode, the temperature setpoint is assumed to be at the typical ice-making temperature of -6°C. In refrigeration mode, the temperature depends on the decided design evaporator temperature differential and design building return temperature, as described below:

$$T^{sw} = T^{rw,des} - \Delta T^{evap,des} \quad (3)$$

where $T^{rw,des}$ is the design return temperature established based on building cooling requirements (10-18°C) and selected coil and $\Delta T^{evap,des}$ is the design evaporator water temperature differential and is a decision variable.

The cooling capacity of a chiller also varies depending on its operating conditions. Changes in the evaporator and condenser temperature from design conditions impact evaporator refrigerant thermal capacity. Modern chillers lose as much as a 30-40% loss in capacity when operating in ice-making mode [19], primarily due to reduced evaporator refrigerant saturation density. Chiller cooling capacity can be estimated from refrigerant thermal capacity resulting in no more than 10% error as described in Reference [15], given known condensing and evaporator temperatures.

Piecewise linearization can then be applied to the determined chiller performance curves. Figure 4 shows the performance curves obtained for a 383-tons Carrier 19XR chiller with a VSD centrifugal compressor in both ice-making and refrigeration modes under three ambient wet-bulb temperatures, overlaid with fitted piecewise linear segments.

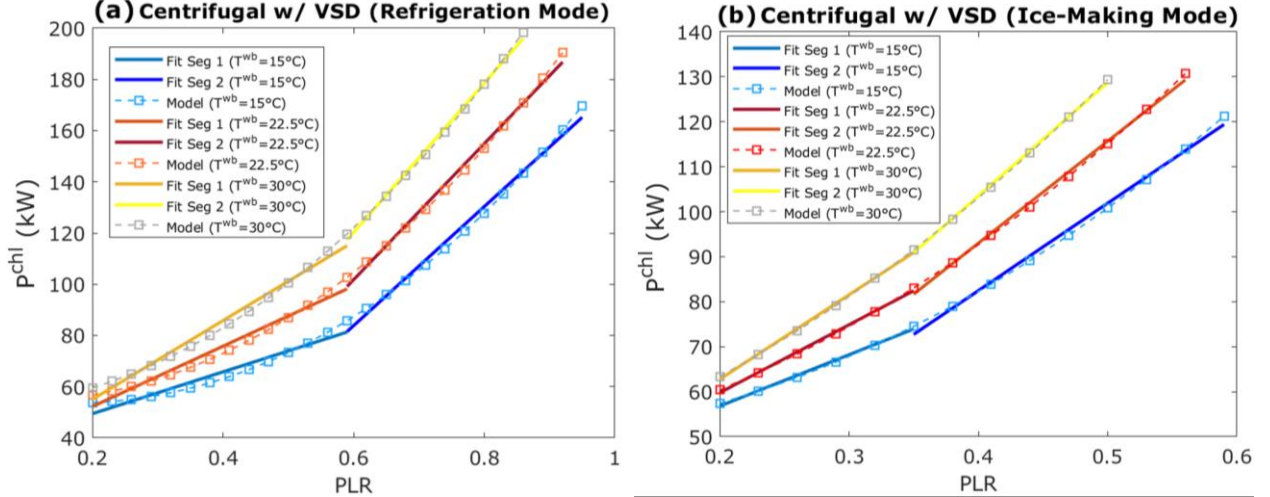


Figure 4: Illustration of piecewise linearization for 383-ton Carrier 19XR chiller with VSD centrifugal compressor under three ambient wet-bulb temperatures in (a) refrigeration mode with a setpoint temperature of 7°C, and (b) ice-making mode with a setpoint temperature of -6°C.

In the simplified mixed-integer linear program formulation, the power use of chillers is determined from the corresponding piecewise linear segment that represents their operating mode, as follows:

$$P_{p,t}^{chl} = \sum_{x \in \mathcal{X}, j \in \mathbb{N}, m \in \mathcal{M}, e \in \mathcal{E}} [a_{p,t,x,j,m,e}^{chl} \dot{Q}_{p,t,x,j}^{chl} + b_{p,t,x,j,m,e}^{chl} B_{p,t,x,j,m,e}^{chl}], \quad \forall p \in \mathcal{P}, \forall t \in \mathcal{T} \quad (4)$$

where subscripts x is the chiller compressor type index set $\{1, 2, 3, \dots\}$ denoted by \mathcal{X} (example is centrifugal without VSD, centrifugal with VSD, ... etc.), and j is the chiller index set $\{1, 2, 3, 4, \dots\}$ such that $j \in \mathbb{N}$, m is the operating mode index set $\{1, 2\}$ denoted by \mathcal{M} and corresponds to 1) refrigeration mode and 2) ice-making mode, and e is the chiller segment index set $\{1, 2\}$ denoted by \mathcal{E} , $\dot{Q}_{p,t,x,j}^{chl}$ is the chiller load, $a_{x,j,m,e}^{chl}$ and $b_{x,j,m,e}^{chl}$ are the piecewise linearized segment slope and intercept, respectively, and $B_{p,t,x,j,m,e}^{chl}$ is a binary decision variable to toggle on the intercept for the corresponding active segment. The number of active segments is restricted to one by the following constraints:

$$\sum_{m \in \mathcal{M}, e \in \mathcal{E}} B_{p,t,x,j,m,e}^{chl} \leq ON_{p,t,x,j}^{chl}, \quad \forall p \in \mathcal{P}, \forall t \in \mathcal{T}, \forall x \in \mathcal{X}, j \in \mathbb{N} \quad (5)$$

$$Q_{p,t,x,j,m,e}^{chl} \leq PLR_{x,m,e}^{ul} Q_{x,j}^{chl,des} B_{p,t,x,j,m,e}^{chl}, \quad \forall p \in \mathcal{P}, \forall t \in \mathcal{T}, \forall x \in \mathcal{X}, j \in \mathbb{N}, m \in \mathcal{M}, e \in \mathcal{E} \quad (6)$$

$$Q_{p,t,x,j,m,e}^{chl} \geq PLR_{x,m,e}^{ll} Q_{x,j}^{chl,des} B_{p,t,x,j,m,e}^{chl}, \forall p \in \mathcal{P}, \forall t \in \mathcal{T}, \forall x \in \mathcal{X}, j \in \mathbb{N}, m \in \mathcal{M}, e \in \mathcal{E} \quad (7)$$

The activated segment is dictated by the decided chiller load that falls within the segment's upper loading limits, $PLR_{x,m,e}^{ul}$, and lower loading limits, $PLR_{x,m,e}^{ll}$. Chillers are restricted to operating in ice-making mode when storing ice and in refrigeration mode (includes storage discharging) otherwise, as described by the following two constraints:

$$\sum_{x \in \mathcal{X}, j \in \mathbb{N}, e \in \mathcal{E}} B_{p,t,x,j,m,e}^{chl} \leq N^{chl} (1 - B_{p,t}^{ice}), \forall p \in \mathcal{P}, \forall t \in \mathcal{T}, m = 1 \quad (8)$$

$$\sum_{x \in \mathcal{X}, j \in \mathbb{N}, e \in \mathcal{E}} B_{p,t,x,j,m,e}^{chl} \leq N^{chl} B_{p,t}^{ice}, \forall p \in \mathcal{P}, \forall t \in \mathcal{T}, m = 2 \quad (9)$$

N^{chl} is the total number of chillers and $B_{p,t}^{ice}$ is a binary variable that toggles ice-making. The total cooling provided by operating chillers is summed up in the following constraint:

$$\dot{Q}_{p,t}^{chl,tot} = \sum_{x \in \mathcal{X}, j \in \mathbb{N}, m \in \mathcal{M}, e \in \mathcal{E}} \dot{Q}_{p,t,x,j}^{chl}, \forall p \in \mathcal{P}, \forall t \in \mathcal{T} \quad (10)$$

Pumps and fans

Pumps continuously transport water to absorb and reject heat to maintain indoor comfort. Chiller pumps (primary and condenser) are fixed-speed pumps controlled to maintain the design water flowrates and only operate with their associated chiller. Conversely, secondary pumps are speed-controlled to deliver the required flowrate to satisfy the building cooling load. The power consumed by pumps is a function of the flowrate and the required pressure head; the two parameters are related by affinity laws. A more efficient pumping configuration can be achieved by reducing the flowrate, which is cubically related to power. However, the reduction of flowrates increases the temperature differential, which comes at the expense of increased chiller power as the supply temperature must be reduced to offset reduced flowrates. An analysis by chillers manufacturer Trane finds that reducing flowrates on both the supply and condenser sides often offsets and compensates for increased chiller energy use [20] and is worthy of consideration in the design problem. The required power by the chillers' pumps is inversely cubically related decided temperature differential and hence flowrate, as described below:

$$P_{p,t}^p = \sum_{x \in \mathcal{X}, j \in \mathbb{N}} \left[P_{x,j}^{pp,des} \left(\frac{\Delta T^{evap,ref}}{\Delta T^{evap,des}} \right)^3 + P_{x,j}^{cp,des} \left(\frac{\Delta T^{cond,ref}}{\Delta T^{cond,des}} \right)^3 \right] \cdot ON_{p,t,x,j}^{chl}, \forall p \in \mathcal{P}, \forall t \in \mathcal{T} \quad (11)$$

Superscripts pp and cp refer to primary and condenser pumps, respectively, ref and des refer to parameters at reference and design conditions, and k is the pump constant at the reference temperature differential. $\left(\frac{\Delta T^{evap,ref}}{\Delta T^{evap,des}} \right)^3$ and $\left(\frac{\Delta T^{cond,ref}}{\Delta T^{cond,des}} \right)^3$ adjust the evaporator and condenser

pumping power for changes in flowrate from reference conditions (reference conditions are as supplied by the manufacturer), respectively. Ideally, the cooling coils fans and secondary pumps' power use varies cubically with the cooling demand per the affinity laws, as follows:

$$P_{p,t}^{dist} = \left(\frac{\dot{Q}_{p,t}^D}{\max_{p \in \mathcal{P}, t \in \mathcal{T}} [\dot{Q}_{p,t}^D]} \right)^3 [P^{sp,des} \left(\frac{\Delta T^{evap,ref}}{\Delta T^{evap,des}} \right)^3 + P^{cf,des}], \quad \forall p \in \mathcal{P}, \forall t \in \mathcal{T} \quad (12)$$

where $\dot{Q}_{p,t}^D$ is the cooling demand, $P^{sp,des}$ and $P^{cf,des}$ are the coil and secondary pump power use when running at design speed. The decided design evaporator temperature differential adjusts the secondary pumps' power use as well per the affinity laws. Using a water-glycol mixture in the supply loop increases pumping power by 15% due to increased viscosity [21].

The power consumed by the cooling tower fan is assumed to vary with the chiller load analogous to fixed-speed fans and is given by:

$$P_{p,t}^{twr} = P^{twr,des} \frac{\dot{Q}_{p,t}^{chl,tot}}{\sum_{x \in \mathcal{X}, j \in \mathcal{N}} \dot{Q}_{x,j}^{chl,des}}, \quad \forall p \in \mathcal{P}, \forall t \in \mathcal{T} \quad (13)$$

where $P^{twr,des}$ is the power consumed by the tower when fans are running at design speed. Although the power varies cubically with the flowrate and is minorly impacted by the COP of the chiller, the simplification is not expected to produce a significant error; the cooling tower power use is small relative to chillers and other auxiliary equipment power use. The power consumed by all auxiliary devices is summed in the following equation:

$$P_{p,t}^{aux} = P_{p,t}^p + P_{p,t}^{dist} + P_{p,t}^{twr}, \quad \forall p \in \mathcal{P}, \forall t \in \mathcal{T} \quad (14)$$

I-TES

I-TES stores energy mainly in the form of latent heat. A popular type of I-TES is internal melt favored for its modularized construction with predictable charge and discharge rates. For this type, the water-glycol mixture received from the chiller is circulated through an internal circuit to freeze or melt the water inside the tank without direct contact, as illustrated in Figure 5. The tank consists of many parallel circuits and is controlled by regulating the inlet temperature and flowrate.

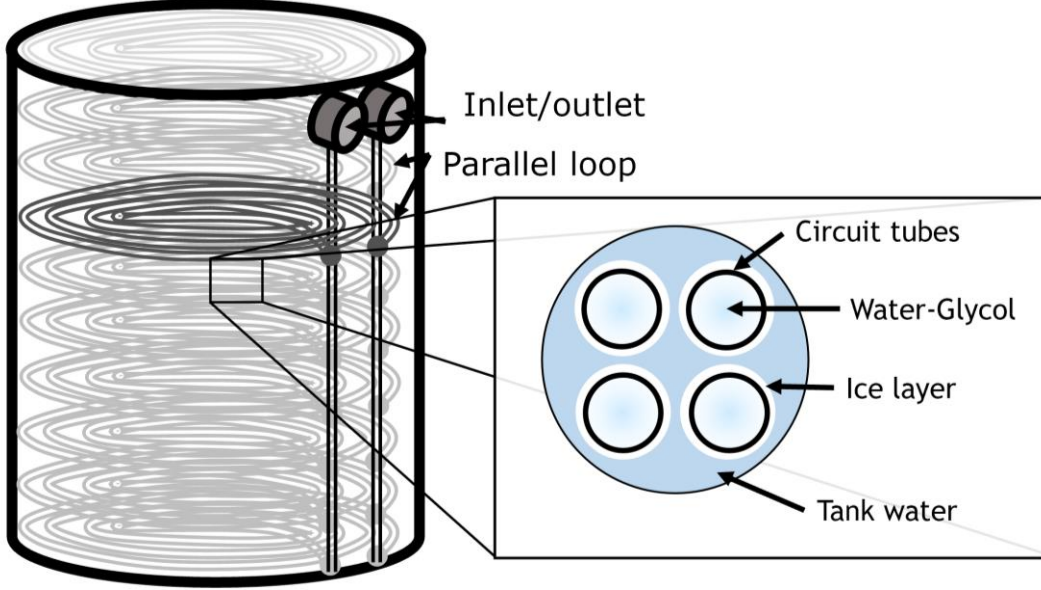


Figure 5: An illustration of a modular internal melt I-TES. Multiple parallel circuits are submerged in water inside the tank, and a water-glycol mixture is circulated through the circuits to build and melt the ice around the tubes.

Albeit predictable, the charge and discharge rates are a complex function of entering water-glycol temperature, flowrate, and the current state of charge. The charge rate is highest during sensible charging enabled by a relatively large temperature differential between the received water-glycol mixture and the average tank water temperature. Once the water begins to freeze, the rate reduces as built-up ice introduces thermal resistance. Likewise, the discharging rate is initially higher when the tank is fully frozen due to the large temperature differential. The rate reduces as the ice melts, and the formed water layer around the tubes warms up, raising the thermal resistance.

The complex behavior of internal melt I-TES is well captured in a model developed by Drees [22] adopted for this work. The performance curves can be simplified to merely a function of the state of charge when the inlet temperature and flowrate are pre-determined. The temperature of the water-glycol mixture received by I-TES is determined based on the chiller operation, as stated earlier. When setting the flowrate to the maximum available flowrate, the maximum heat rates are attained, which are used to limit the storage charge and discharge rates. The maximum available flowrate is the total flowrate when all chillers are operating, limited to the flowrates the storage can tolerate as follows:

$$\dot{m}^{iw} = \min[\dot{m}^{iw,max}, \sum_{x \in \mathcal{X}, j \in \mathbb{N}} \dot{m}_{x,j}^{sw}], \forall p \in \mathcal{P}, \forall t \in \mathcal{T} \quad (15)$$

where $\dot{m}^{iw,max}$ is the maximum flowrate the I-TES tank is designed to tolerate. Piecewise linearization is then applied to the determined maximum charge/discharge rates and is given by:

$$S_{p,t,f,m}^{lim} \leq a_{f,m}^S \left(\frac{S_{p,t}}{C^{ITES}} \right) + b_{f,m}^S B_{p,t,f,m}^{ITES} + M(1 - B_{p,t,f,m}^{ITES}), \quad \forall p \in \mathcal{P}, \forall t \in \mathcal{T}, f \in \mathcal{F}, m \in \mathcal{M} \quad (16)$$

$$S_{p,t,f,m}^{lim} \leq M B_{p,t,f,m}^{ITES}, \quad \forall p \in \mathcal{P}, \forall t \in \mathcal{T}, f \in \mathcal{F}, m \in \mathcal{M} \quad (17)$$

where subscripts f is the I-TES segment index set $\{1, 2\}$ denoted by \mathcal{F} , $a_{f,m}^S$ and $b_{f,m}^S$ are the piecewise linearized slope and intercept, respectively, M is an arbitrarily large number (Big-M), and C^{ITES} is the installed net usable I-TES capacity. The total net usable I-TES capacity is based on the decided supply setpoint temperature in refrigeration mode, which dictates the sensible thermal capacity and is responsible for deviations from nominal capacity. $B_{p,t,f,m}^{ITES}$ is a binary decision variable to toggle the corresponding piece-wise segments based on the operating mode depending on the state of charge, as follows:

$$S_{p,t} \leq SoC_{f,m}^{ul} C^{ITES} B_{p,t,f,m}^{ITES}, \quad \forall p \in \mathcal{P}, \forall t \in \mathcal{T}, f \in \mathcal{F}, m \in \mathcal{M} \quad (18)$$

$$S_{p,t} \geq SoC_{f,m}^{ll} C^{ITES} B_{p,t,f,m}^{ITES}, \quad \forall p \in \mathcal{P}, \forall t \in \mathcal{T}, f \in \mathcal{F}, m \in \mathcal{M} \quad (19)$$

where $SoC_{f,m}^{ul}$ and $SoC_{f,m}^{ll}$ are the upper and lower limits state of charge for each segment. The following constraints limit the number of active segments to one at each time step:

$$\sum_{f \in \mathcal{F}} B_{p,t,f,m}^{ITES} = 1, \quad \forall p \in \mathcal{P}, \forall t \in \mathcal{T}, m \in \mathcal{M} \quad (20)$$

The decided storage charge/discharge rates are limited to the computed maximum rates. However, since the analysis is done on an hourly basis in which the storage maximum charge/discharge rate can change considerably, the decided rates are restricted based on the average rate between the maximum rate at the current and next-time step state of charge, as follows:

$$S_{p,t}^{chs} \leq \sum_{f \in \mathcal{F}} \left[\frac{1}{2} (S_{p,t,f,m}^{lim} + S_{p,t+1,f,m}^{lim}) \right], \quad \forall p \in \mathcal{P}, \forall t \in \mathcal{T}, m = 1 \quad (21)$$

$$S_{p,t}^{dis} \leq \sum_{f \in \mathcal{F}} \left[\frac{1}{2} (S_{p,t,f,m}^{lim} + S_{p,t+1,f,m}^{lim}) \right], \quad \forall p \in \mathcal{P}, \forall t \in \mathcal{T}, m = 2 \quad (22)$$

$S_{p,t}^{chs}$ and $S_{p,t}^{dis}$ are the I-TES decided charge and discharge rates, respectively. I-TES is constrained to either be in charging or discharging mode, which is dictated by the chiller operating mode, as described by the following constraints:

$$S_{p,t}^{chs} \leq M B_{p,t}^{ice}, \quad \forall p \in \mathcal{P}, \forall t \in \mathcal{T} \quad (23)$$

$$S_{p,t}^{dis} \leq M(1 - B_{p,t}^{ice}), \quad \forall p \in \mathcal{P}, \forall t \in \mathcal{T} \quad (24)$$

Figure 6 shows the I-TES charge rate curve in (a) and discharge rate curve in (b) overlaid with piecewise linear segments for the CALMAC 83-ton-hr ice tank. The discharge rate curve is well captured with three segments while four segments are needed for the charge rate curve and they overlap with the previously discussed stages of charging and discharging. The amount of stored thermal energy in I-TES is balanced in the following constraint:

$$S_{p,t} - \eta^{ITES,sdis} S_{p,t-1} = S_{p,t}^{chs} - S_{p,t}^{dis}, \quad \forall p \in \mathcal{P}, \quad \forall t \in \mathcal{T} \quad (25)$$

where $\eta^{ITES,sdis}$ is the I-TES self-discharge efficiency.

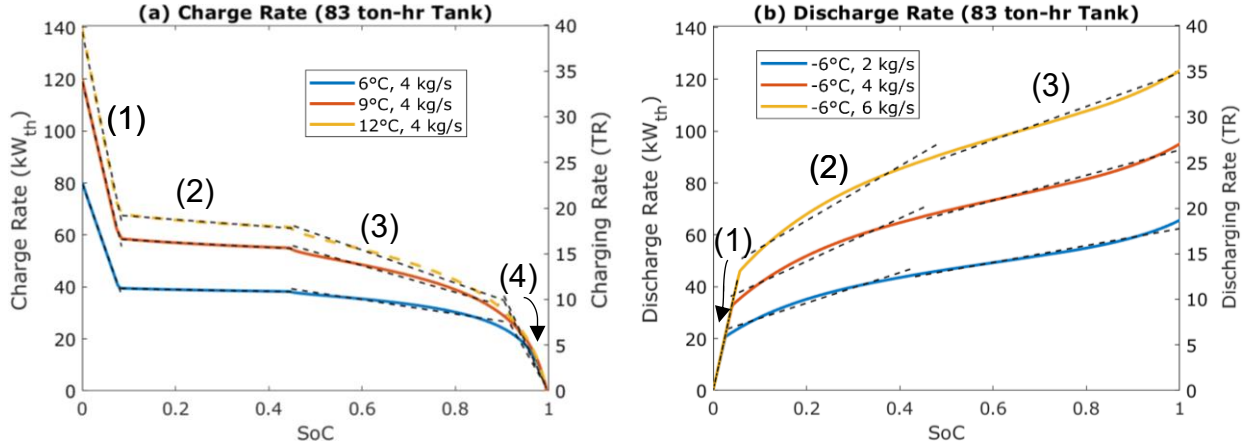


Figure 6: Piecewise linearized charge and discharge rates for CALMAC 83-ton-hr I-TES.

BESS

BESS maximum charge and discharge rates are a function of the state of charge and are affected by degradation. However, the performance can be well captured using a linear model with constant efficiencies [10]. No considerations need to be made for depth of discharge when taking BESS capacity, C^{BESS} , as the net usable capacity. Charge and discharge rates are restricted based on typical 4-hour batteries with a power-to-energy capacity ratio of 1/4. The subsequent three constraints balance the stored energy and limit charge/discharge rates:

$$\mathcal{B}_{p,t}^s - \eta^{BESS,sdis} \mathcal{B}_{p,t-1}^s = \eta^{BESS,chs} \mathcal{B}_{p,t}^{chs} - \frac{1}{\eta^{BESS,dis}} \mathcal{B}_{p,t}^{dis}, \quad \forall p \in \mathcal{P}, \quad \forall t \in \mathcal{T} \quad (26)$$

$$\mathcal{B}_{p,t}^s \leq C^{BESS}, \quad \forall p \in \mathcal{P}, \quad \forall t \in \mathcal{T} \quad (27)$$

$$\mathcal{B}_{p,t}^{chs} + \mathcal{B}_{p,t}^{dis} \leq \left(\frac{1}{4}\right) \times C^{BESS}, \quad \forall p, \forall t \quad (28)$$

where $\mathcal{B}_{p,t}^{chs}$ and $\mathcal{B}_{p,t}^{dis}$ are BESS charge and discharge rates, respectively, $\mathcal{B}_{p,t}^s$ is the stored electric energy and $\eta^{BESS,sdis}$, $\eta^{BESS,chs}$, and $\eta^{BESS,dis}$ are the self-discharge, charge, and discharge

efficiencies, respectively. Solutions with simultaneous charging and discharging are eliminated by adding a small cost in the order of 10^{-3} \$/MW to $\mathcal{B}_{p,t}^{chs}$ in the lower-level objective function, which does not impact the cost-optimal system.

2.3 Problem formulation

The objective is to minimize annual system costs from Capex and OpEx by utilizing lower-cost PV generation which reduces carbon emissions. The main cost function that is to be minimized by the upper-level optimizer is as follows:

$$\begin{aligned} \min Cost = & c^{BESS} C^{BESS} \frac{ir(ir+1)^{yrb}}{(1+ir)^{yrb}-1} + [c^{PV} C^{PV} + c^{ITES} C^{ITES} + \sum_{x \in \mathcal{X}, j \in \mathbb{N}} c_x^{chl} Q_{x,j}^{chl,des} + \\ & \sum_{x \in \mathcal{X}, j \in \mathbb{N}} c^{P,FS} C_{x,j}^p + c^{P,VSD} C^{sp} + c^{twr} C^{twr}] \frac{ir(ir+1)^{yr}}{(1+ir)^{yr}-1} + c^{PV,O} C^{PV} + OpEx \end{aligned} \quad (29)$$

where OpEx is the estimated yearly electricity charge as determined by solving the scheduling and dispatch problem in the lower level. The lower-level objective function is given by:

$$\min OpEx = \sum_{p \in \mathcal{P}, t \in \mathcal{T}} c_t^e G_{p,t} N_p^{days} + c^P \sum_{p \in \mathcal{P}} G_p^P N_p^{mos} \quad (30)$$

$c^e \sum_{p \in \mathcal{P}, t \in \mathcal{T}} G_{p,t} N_p^{days}$ and $c^P \sum_{p \in \mathcal{P}, t \in \mathcal{T}} G_{p,t} N_p^{mos}$ are the electricity charges from energy use and demand charges, respectively. c_x^{chl} , c^{PV} , c^{BESS} , c^{ITES} , $c^{P,FS}$, $c^{P,VSD}$, c^{twr} are installed chillers, PV, BESS, I-TES, chiller pumps, secondary pumps, and cooling towers Capex, respectively, and C^{PV} , C_j^p , C^{sp} , C^{twr} are the installed PV, chiller pumps, secondary pumps, and cooling towers capacities, respectively, $G_{p,t}$ is the electricity consumed from the grid, G_p^P is peak electricity demand, N_p^{days} and N_p^{mos} are the number of days (to compute hourly electricity use and charges) and months (to compute monthly demand charges) represented by scenario p , respectively, c_t^e and c^P are hourly electricity tariffs and peak demand charges, respectively, $c^{PV,O}$ is the yearly OpEx for installed PV, ir is the interest rate, yrb is the BESS's service life, and yr is the service life of all other equipment.

The installed fixed and variable speed pumps capacities are the pumps' rated power, as described by the following two equations:

$$C_{x,j}^p = P_{x,j}^{cp,des} + P_{x,j}^{pp,des} \quad (31)$$

$$C^{sp} = p^{sp,des} \quad (32)$$

The cooling towers are sized to reject the heat generated when all chillers are operating at their design capacity, as follows:

$$C^{twr} = \frac{\Delta T^{cond,ref}}{\Delta T^{cond,des}} \sum_{x \in \mathcal{X}, j \in \mathbb{N}} Q_{x,j}^{chl,des} \left(1 + \frac{1}{COP_{x,j}^{ref}} \right) \quad (33)$$

The size of the cooling towers and hence their cost is approximated to vary linearly with the water flowrate relative to reference conditions. Reduced flowrates reduce the required fill area inside the tower.

The upper-level optimization is only constrained by a minimum and maximum chiller capacity:

$$\underline{Q}^{chl,des} \leq Q_{x,j}^{chl,des} \leq \overline{Q}^{chl,des} \quad (34)$$

$\underline{Q}^{chl,des}$ and $\overline{Q}^{chl,des}$ are the preferred lower and upper limits for the nominal chillers' capacity decision variables. It is restricted to reduce the risk of loss of service due to downtime and maintenance.

Three constraints apply to the lower-level problem. The first lower-level constraint balances the building electricity demand and supply, as follows:

$$P_{p,t}^{chl} + P_{p,t}^{aux} + B_{p,t}^{chs} + PV_{p,t}^{curt} + \mathcal{L}^{Elec} = \eta^I I_{p,t} C^{PV} + B_{p,t}^{dis} + G_{p,t}, \quad \forall p \in \mathcal{P}, \forall t \in \mathcal{T} \quad (35)$$

where $PV_{p,t}^{curt}$ is the curtailed PV generation, \mathcal{L}^{Elec} is the building's non-cooling load, and $I_{p,t}$ is the incident solar insolation on an inclined surface at the optimal fixed-tilt angle. Chillers' cooling supply and I-TES dispatch amount are balanced with the cooling demand in the following constraint:

$$\dot{Q}_{p,t}^{chl,tot} + S_{p,t}^{dis} = \dot{Q}_{p,t}^D + S_{p,t}^{chs}, \quad \forall p \in \mathcal{P}, \forall t \in \mathcal{T} \quad (36)$$

Since the first hour of the day is an arbitrary decision, the storage can have a non-zero initial state of charge given that it matches the end-of-day state of charge, as described by the following constraint:

$$S_{p,t=1} = S_{p,t=24}, \quad \forall p \in \mathcal{P} \quad (37)$$

2.4 Simulation of building cooling and electric loads

Buildings' cooling load is influenced by the interaction of weather with the buildings' envelope, occupancy and occupants' activity level, and electric loads. In the literature, simulation methods of building cooling load can be classified into three categories [23]: (i) energy simulation models, (ii) data-driven models, and (iii) hybrid models. Energy simulation models are performed using software tools such as EnergyPlus, TRANSYS, and eQuest. They require complete knowledge of building envelope construction, orientation, and materials [24,25]. They are often used for more sophisticated estimations of cooling loads that are not necessary to validate the model in this paper. Data-driven models drive patterns from historical data using meteorological and occupancy data [26,27], which Qatar lacks. On the other hand, hybrid models use parameters that simplify the building description in energy models and are used in optimization problems [28,29]. This paper uses the hybrid model approach to simulate a building cooling load profile. The intention is to capture the diurnal and interannual demand profile for a generic building in Qatar without an explicit description of the building's interior zoning, orientation, and construction details.

The cooling load for a high-rise building (30 stories; gross floor area of 60,000 m²; square floor area) is simulated using heat balance equations in a hybrid model. The simulation of cooling load is accomplished by adding heat gains from all major sources, including (i) occupant metabolic heat generation rate, (ii) electric load, (iii) introduction of outdoor air from infiltration and ventilation, (iv) solar gain through fenestration, and (v) heat gain through the building envelope. Several assumptions are made to estimate the heat gain from each source. The assumptions, in no order, are as follows:

General:

- The building interior is maintained at 22°C and 50% relative humidity at all times.
- Building occupancy is assumed based on typical working hours in Qatar.
- Building non-cooling electric load is calculated based on assumed occupancy and typical electric energy consumption rates in residential settings (75 kWh/m²/yr.[30]).
- Occupant activity level is assumed to be primarily resting.
- Cooling demand is simulated hourly using meteorological data from Doha International Airport

Building construction:

- The building consists of 30 floors with a square area of 2000 m² and a height of 3 m.

- 30% of the building façade is covered with glazing, which is on par with typical high-rise buildings worldwide and in Qatar.
- No specific building orientation is supposed; instead, one side of the building envelope is assumed to be always directly facing the sun when estimating the thermal gain from admitted solar irradiation.
- Building thermal insulation is on par with Qatar's building code (overall heat transfer coefficients of $0.6 \text{ W/m}^2\text{-K}$ for all exterior walls, $1.8 \text{ W/m}^2\text{-K}$ for all windows, and $0.6 \text{ W/m}^2\text{-K}$ for the upper-most roof) with exterior surfaces at the ambient temperature.
- The combined infiltration and ventilation rate for the entire building is 1.25 ACH (air change per hour), which is on par with typical modern construction and Qatar [31].

The estimated non-cooling electric load serves two purposes: (i) it measures the contribution to the building's thermal load, and (ii) it represents the building's non-cooling electricity demand. The non-cooling electric load is influenced by building use, occupancy, and time of day. Household electricity consumption in Qatar has only been reported in the literature a few times [5,32,33]. Demand spikes are observed in the morning between 5 and 7 AM, late afternoon between 3 and 5 PM, and evening between 6 and 9 PM, which correlates with building occupancy. These reported demand profiles are used in deriving an estimate for the building's non-cooling electric load, shown in Figure 7. The load is characterized by a pre-work morning spike, a post-work evening spike, and a generally higher evening load. The average daily electric load is 515 kW (8.6 W/m^2).

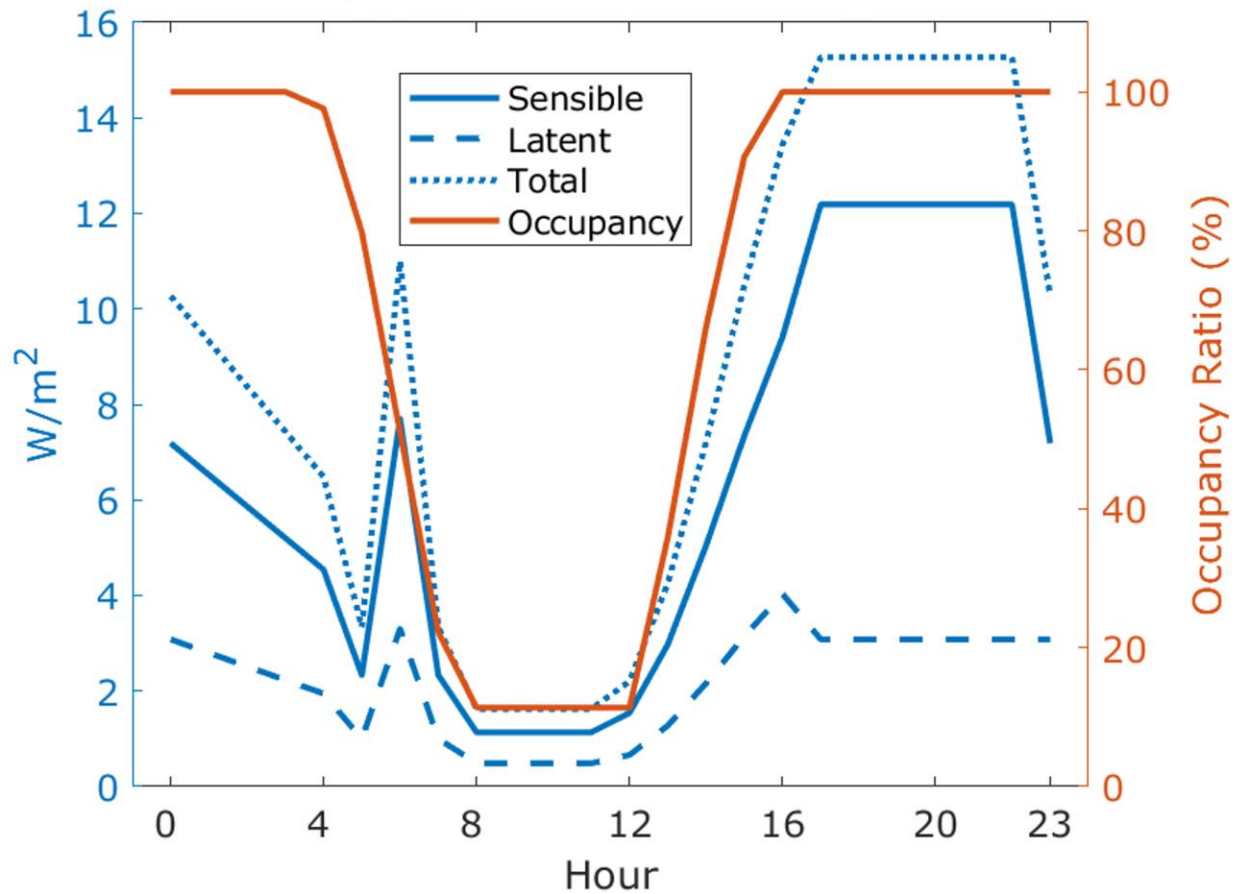


Figure 7: Estimated residential building non-cooling electric load.

The simulated buildings' main heat gain sources are infiltration and ventilation, followed by internal generation from electricity use. Loads from internal sources drive daily variations, while seasonal variations are driven by infiltration and ventilation heat gain, particularly from latent load during the summer from late July to early September. These daily differences impact the storage capacity needed for load shifting. Figure 8 shows the simulated building cooling loads for three days in winter (January 5-7), spring (April 10-12), and summer (September 2-4) representative of their respective season. The yearly cooling need is 19.5 GWh_{th} (325 kWh_{th}/m²), and electricity consumption is 4.5 GWh (75 kWh/m²) using Doha's 2016 hourly meteorological data. The subscript "th" is used to differentiate between cooling and electric energy demand. The resultant estimated building cooling intensity (cooling load normalized by floor area) agrees with the data reported in the literature when assuming a standard AC system COP (coefficient of performance) of 2.5-3 [5,32].

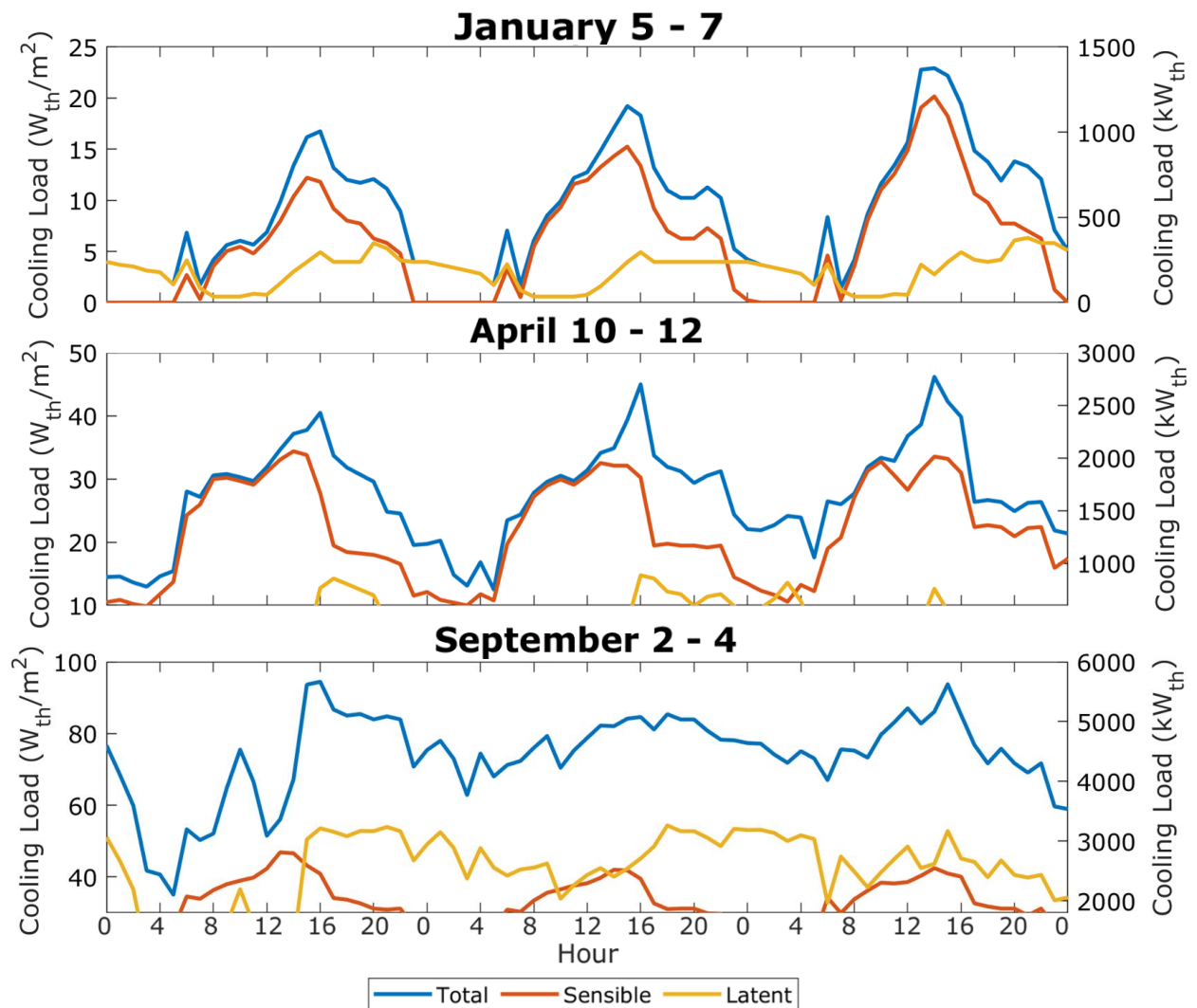


Figure 8: Simulated residential building cooling load for three days in winter, spring, and summer. Electric and thermal loads are correlated with higher building occupancy in the evening.

2.5 Scenarios selection

Five scenarios are selected from the hourly simulated cooling demand. Four scenarios represent a typical day in each season to capture the intra-annual demand and weather variations in addition to the peak demand day scenario. The five selected scenarios are tabulated in Table 1.

Table 1: Selected scenarios

Scenario	Date	Number of Represented Days (days/yr.)
1 Design day	August 15	10
2 High cooling	July 28	76
3 Moderate cooling	July 11	109
4 Shoulder Season	March 13	101
5 Low Cooling	January 30	69

Scenario 1 represents the peak demand or design day, occurring only ten days out of the year. This scenario dictates the minimum installed cumulative chiller and I-TES capacities. Scenario 2 is the high cooling demand period that lasts two months, between mid-July and mid-September, and is driven by the high ambient temperature and humidity levels. Scenario 3 is the moderate cooling season and persists for 109 days a year. This period represents one of the largest parts of the year, from mid-May to mid-July and from mid-September to mid-October. This period is dominated by high peak daytime temperatures between 35 and 45°C, which drives the building cooling load. Scenario 4 is the second longest period representing 101 days out of the year occurring in late fall and early spring. This scenario exemplifies the shoulder season, characterized by moderately warm days with afternoon temperatures between 30 and 35°C. Scenario 5 is the low cooling season with a load primarily driven by occupancy and electricity load. This scenario exemplifies the low cooling season in the winter and is best described by mild daytime temperatures between 20 and 25°C and cool nighttime temperatures between 15 and 20°C.

Figure 9 shows the hourly cooling demand, non-cooling electric demand, solar insolation, and ambient wet-bulb temperature for the five scenarios. The non-cooling load is fixed year-round and is characterized by a morning spike and a higher evening load. The building's peak cooling demand is 6550 kW_{th} and reduces by a factor of 4 to 1500 kW_{th} in the low cooling season.

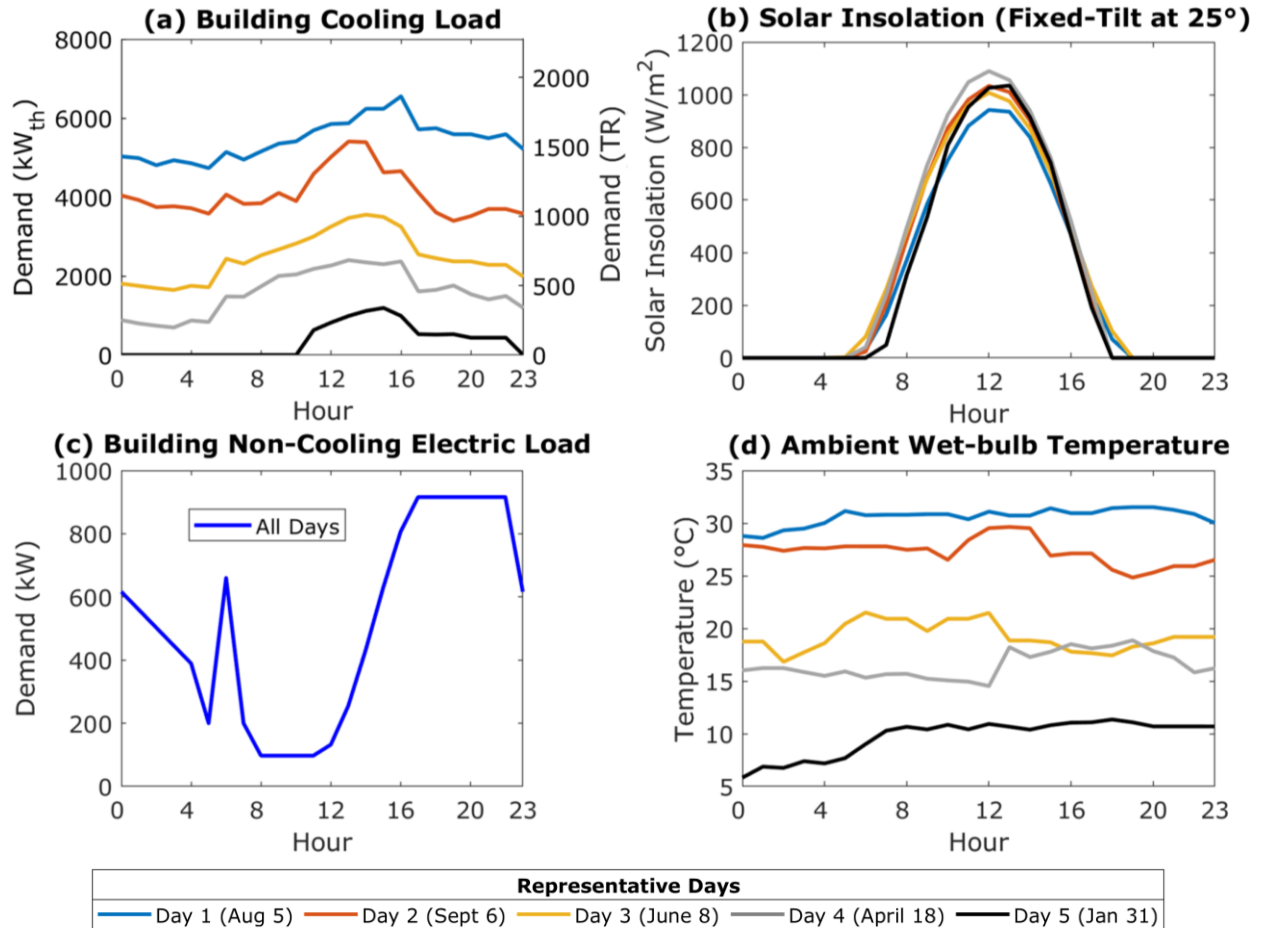


Figure 9: Selected five scenarios with (a) building thermal cooling demand, (b) solar insolation, (c) non-cooling electric load, and (d) ambient wet-bulb temperature.

In Qatar, electricity is subsidized based on sector and consumption bracket [34]. For non-bulk customers (buildings with peak demand less than 5 MW) with monthly consumption of 4 MWh, the rate is flat at \$36/MWh for all sectors and unsuitable for carbon pricing analysis. Instead, unsubsidized bulk customer electricity rates are used, albeit the modeled building falls short of the criteria for bulk customers. The considered tariff structure is tabulated in Table 2. The rate is \$58/MWh during the low-demand seasons and increases to \$93/MWh during peak hours in the higher-demand months (May to October) from 12 to 6 PM [34]. No demand charges are currently implemented in Qatar ($c^p = \$0/\text{MW}_p$).

Table 2: Qatar electricity tariff for bulk customers

Hours	Rates
May 1 – October 31	
12:00 PM – 6:00 PM	\$93/MWh
6:00 PM – 12:00 PM	\$66/MWh
November 1 – April 30	
All day	\$58/MWh

3. Results and discussion

To establish a benchmark, the formulated problem is first solved with building electricity demand being entirely supplied from the grid. The problem is then solved with carbon pricing from 0 to \$150/ton of CO₂ at an increment of \$25/ton of CO₂ to determine the system's annual cost and cost-optimal capacities of on-site PV, BESS, I-TES, and WC CWS. Selection details of the model parameters are in the Appendix. The effect of the carbon price on the cost-optimal system installed capacities is shown in Figure 10, and the corresponding system characteristics are shown in Figure 11. The developed model required reasonable computational resources with an execution time of less than 1 hour (for each given carbon price) using a moderately powerful personal computer. Additionally, the model exhibited stability with consistent convergence.

The cost-optimal system with carbon pricing below \$50/ton of CO₂ is entirely dominated by PV generation with a limited I-TES capacity. The cost of energy storage for highly seasonal cooling needs cannot out-compete low-cost electricity from the grid. This system utilizes PV generation to nearly meet all daytime electricity demand and exploits excess generation in the shoulder seasons to partially meet nighttime cooling demand using I-TES, enabled by a large idle chillers capacity. The model results suggested optimal on-site PV capacity borders the building's peak electricity demand constrained by (i) the lack of feed-in tariff, to reduce curtailments (shown in Figure 11) with highly seasonal loads, (ii) slight misalignment of building demand peak with solar insolation peak, and (iii) cost-prohibitive energy storage with modest carbon pricing. At this carbon pricing, the annual system cost is overwhelmingly dominated by electricity charges.

BESS becomes cost-effective with moderate carbon pricing above \$75/ton of CO₂. The model results indicate that BESS does not replace I-TES for load shifting and is rather mainly used to manage the non-cooling load. BESS's high cost of capacity necessitates near-daily full capacity utilization to be cost-effective, making it particularly unsuitable for highly seasonal loads. Alongside a larger I-TES capacity, they are used to reduce the significant nighttime electricity demand and could reduce emissions by about 50-90% subject to carbon pricing. Furthermore, the model results suggest a rapid increase in installed BESS capacity with carbon prices up to \$100/ton of CO₂. For this system, emissions could be reduced by about 87%, of which PV, BESS, and I-TES contribute 42%, 37%, and 8%, respectively. The annual system cost became predominantly from BESS, accounting for nearly half of the annual system cost. For this system, OpEx is reduced by a factor of 2 relative to a system without carbon pricing; pricier energy from the grid is substituted by investment in PV and BESS.

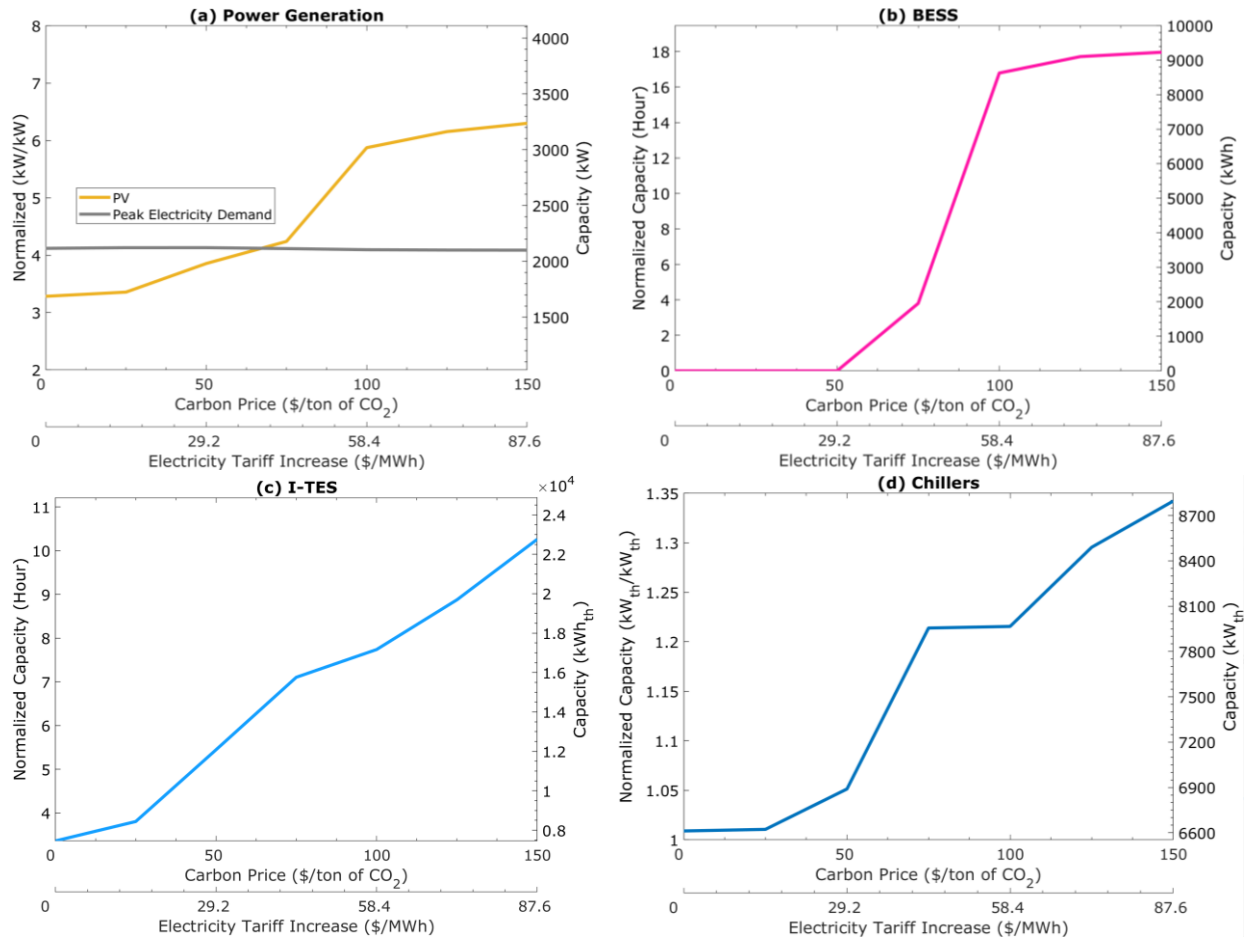


Figure 10: Effect of the carbon price on the cost-optimal system installed capacities of (a) PV, (b) BESS, (c) I-TES, and (d) chillers. PV and BESS are normalized to the average electric demand of 515 kW, I-TES is normalized to the average cooling load of 2213 kW_{th}, and the total capacity of chillers is normalized to the peak cooling demand of 7160 kW_{th}.

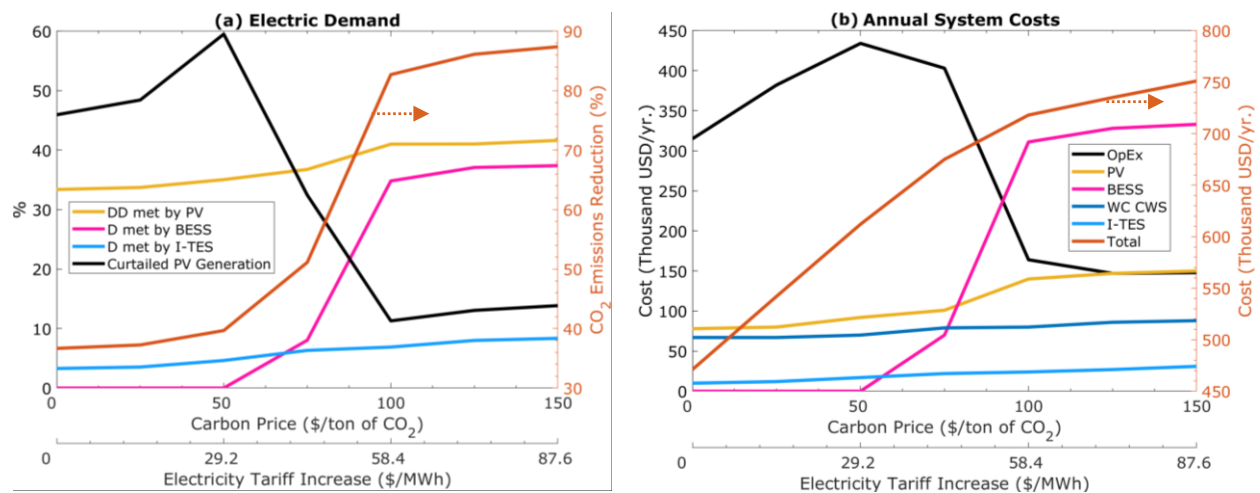


Figure 11: Effect of the carbon price increases on (a) contribution to meeting the electric demand and (b) breakdown of annual system cost.

Meeting nighttime demand during the peak demand season between July and September remains a challenge for this system restricted by the available idle chillers' cooling capacity and the narrow charging window. The available idle chillers' cooling capacity is stressed from capacity degradation in ice-making mode as well as the increased ambient temperatures in the summer. Several possible approaches can alleviate the challenges of decarbonizing a highly seasonal cooling load, including more efficient cooling technologies and more energy-efficient buildings that could reduce the seasonality of the cooling load, and long-term energy storage technologies that could exploit large surplus PV generation in late spring prior to peak cooling season.

The carbon abatement cost as carbon pricing increases and the abated CO₂ are shown in Figure 12. The negative abatement cost with carbon pricing below \$50/ton of CO₂ signifies that a more sustainable solution can be achieved with a reduced annual cost. The mismatch between electricity demand and solar insolation requires energy storage which drives carbon abatement costs to \$40/ton of CO₂. Nevertheless, the abatement cost does not exceed \$50/ton of CO₂ up to a decarbonization rate of nearly 90%, supported by low-cost PV generation combined with the low cost of I-TES with sufficient idle chiller capacity and reliable year-round nighttime electricity demand for BESS. Investment in BESS moderately increases annual system costs by 25% from \$600 thousand/yr. to \$750 thousand/yr. while abating nearly 3000 tons of CO₂/yr. (50% of yearly carbon emissions).

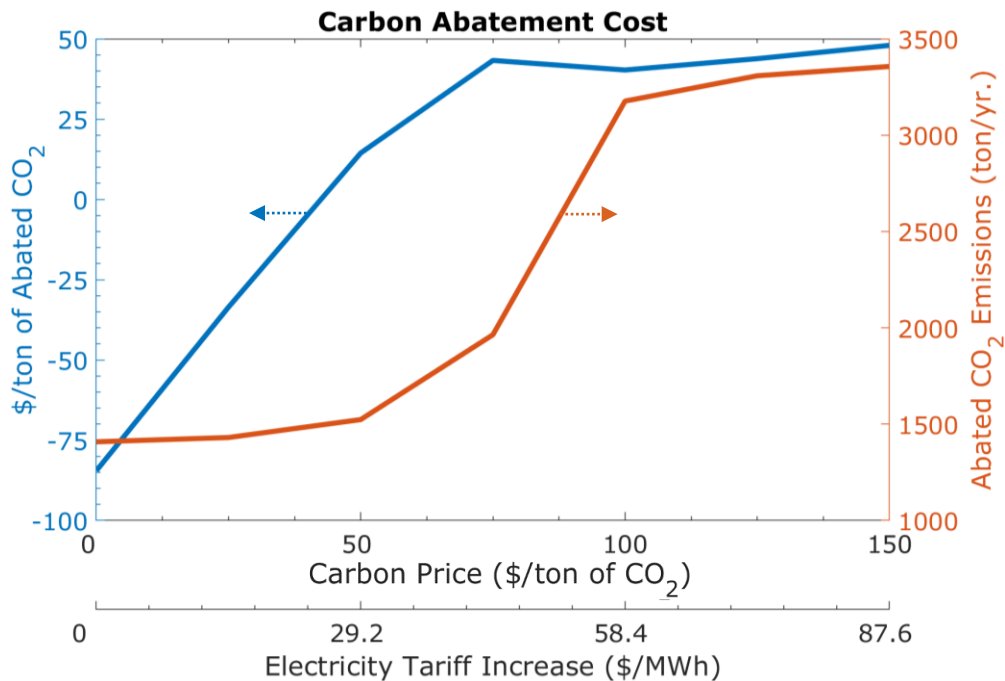


Figure 12: Carbon abatement cost and abated CO₂.

Decided chillers' capacities and types are tabulated in Table 3. The cost-optimal system consists of three chillers, two of which are VSD-equipped centrifugal compressors for optimized part load performance. This selection is supported by the large intra-annual variations in ambient wet-bulb

temperatures in addition to changes in cooling demand during the day. The unequal capacities of centrifugal chillers with VSD allow for more efficient chiller sequencing and reduced pump power use as the load fluctuates over the seasons. This configuration is especially important since chillers are often part-loaded, whereas their associated pumps' power use is constant. The third chiller is a lower-cost screw chiller that supports I-TES charging and supplements cooling during the short-lived high-cooling demand season. Furthermore, a relatively larger VSD chiller capacity and a smaller screw chiller are selected at a low carbon tax. The difference in selection is attributed to reduced needs for I-TES charging and slightly enhanced part-load performance of the larger chiller.

On par with recommendations by the prominent chillers manufacturer, Trane [20], the decided design temperature differential in the evaporator for all scenarios is 8°C. The temperature is sufficient enough to reduce pumps energy use yet not large enough to overwhelm the chillers. The decided temperature differential on the condenser side is higher at 10°C, which reduces condenser pump power use and the size of the cooling tower. Although it degrades the chillers' cooling capacity, the oversized cooling capacity compensates for the degradation.

Hourly chillers loading and load profile for Scenarios 2-4 for a system without carbon pricing are shown in Figure 13, and for a system with a carbon price at \$100/ton of CO₂ are shown in Figure 14. A large amount of PV generation is curtailed, especially in the low-cooling demand season. However, as carbon pricing increases and BESS becomes cost-effective, most excess of the generation is utilized to meet nighttime electricity needs. Lastly, the increase in cumulative chiller capacity with higher carbon pricing enables a larger contribution from I-TES.

Table 3: Optimal-cost cooling system I-TES and chillers' capacities

Carbon Price (\$/ton of CO ₂)	CWS Cost (Thousand \$/yr.)	I-TES Capacity (kWh _{th})	Chiller 1 (VSD Centrifugal) (kW _{th})	Chiller 2 (VSD Centrifugal) (kW _{th})	Chiller 3 (Fixed Speed Screw) (kW _{th})	Total Chiller Capacity (kW _{th})
Base	67	0	3,165	2,269	1,145	6,580
0	67	7,457	3,165	1,925	1,521	6,612
25	68	8,441	3,165	2,065	1,391	6,621
50	70	12,081	3,165	1,963	1,761	6,889
75	79	15,760	3,165	1,721	3,071	7,956
100	80	17,165	3,165	2,051	2,751	7,967
125	86	19,687	3,165	3,127	2,197	8,490
150	88	22,758	3,165	2,922	2,708	8,796

\$0/ton of CO₂

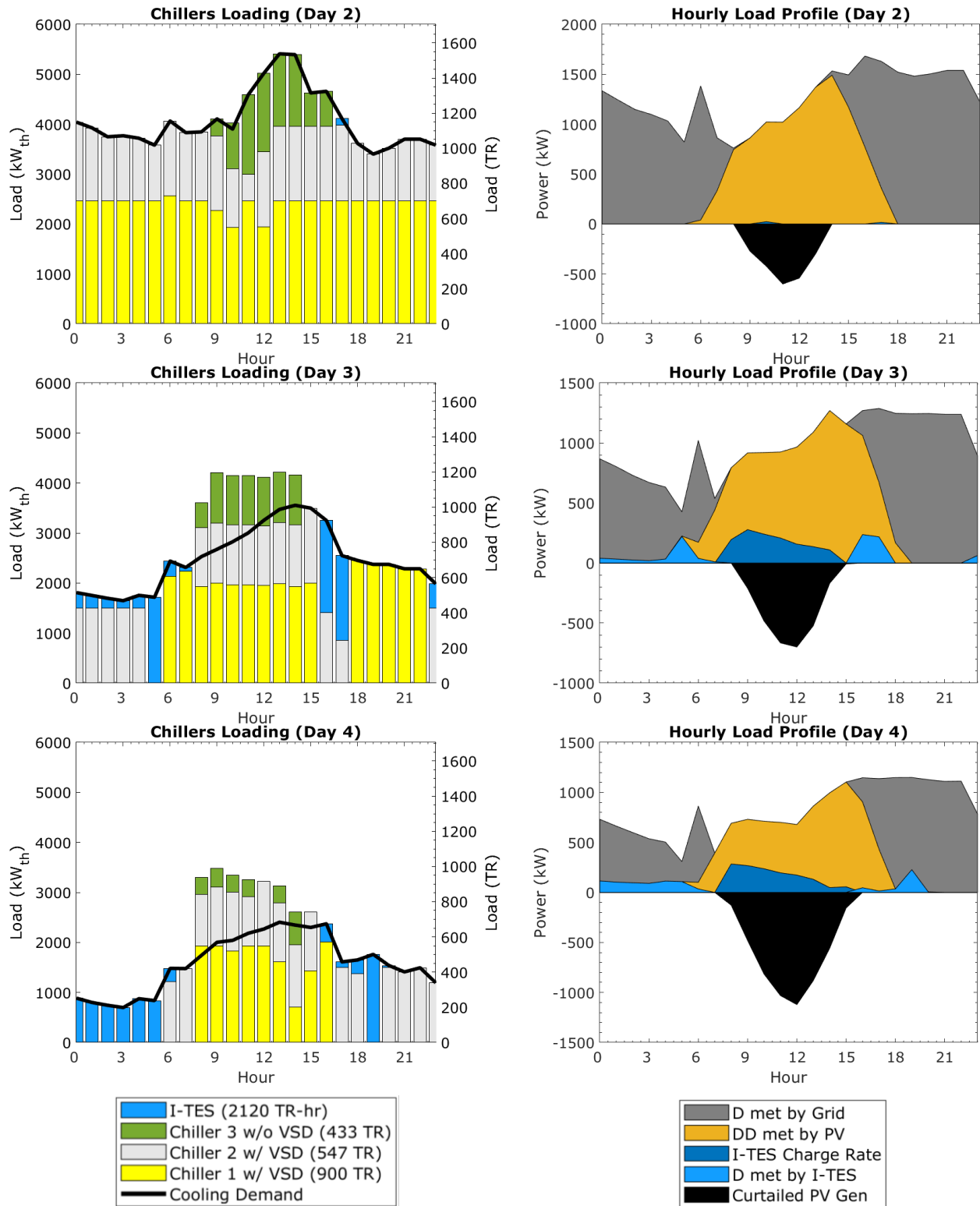


Figure 13: Cost-optimal system with (a) chillers loading and (b) hourly load profile without carbon pricing.

\$100/ton of CO₂

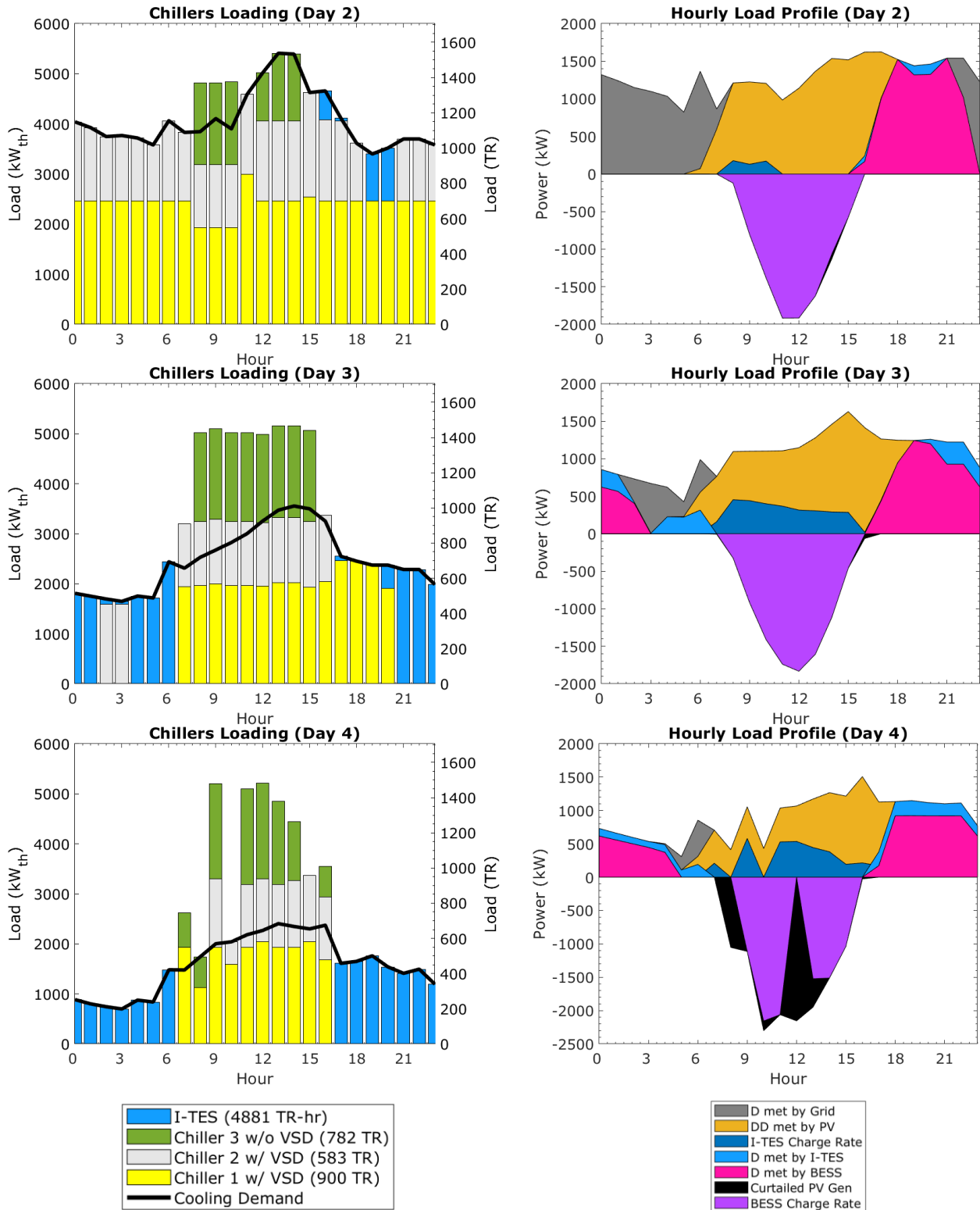


Figure 14: Cost-optimal system with (a) chillers loading and (b) hourly load profile with carbon pricing at \$100/ton of CO₂.

4. Conclusion

Limiting global warming to 1.5°C requires transitioning to low-carbon electricity grids. High and predictable solar insolation in arid regions synergetic with cooling demand is attractive for exploiting PV-enabled decarbonization solutions. This paper examines a building-scale decarbonization solution using an integrated multi-chiller system with I-TES, BESS, and PV. The paper proposes an optimization strategy for system design that negates the need for simplistic models that are widely used in the literature. The strategy decides multi-chiller capacities and types while accounting for their part-load performance and the impact of intra-annual ambient temperature variations.

The developed strategy simplifies the problem into a bi-level optimization formulation to decouple the equipment capacity sizing problem from the complex scheduling and dispatch problem. The upper level minimizes yearly total system costs and decides the installed capacities and design parameters using particle swarm optimization. The decided parameters are used to build and solve a mixed-integer linear model of the scheduling and dispatch problem with piecewise linearized equipment performance curves. The estimated operating costs from solving the lower-level problem are used to adjust the next iteration guesses. Physics-based models of the main power-consuming devices were used as a foundation to build piecewise linearized component models.

To evaluate the developed solution strategy and decarbonization solution, the model was applied to a generic residential building in Qatar and exposed to a range of carbon pricing to accelerate the adoption of sustainable energy resources. Due to the lack of building demand profiles, the cooling load is simulated for generic residential buildings representative of the residential building stock. The model results affirm the suitability of the proposed system; residential buildings are positioned to nearly eliminate emissions from electricity use with moderate carbon pricing between \$75 and \$125/ton of CO₂. I-TES is suitable for utilizing the large idle chiller capacities during the shoulder cooling season for load shifting. However, load shifting using I-TES in the high cooling season remains a challenge because of (i) chiller capacity degradation due to ice-making as well from higher ambient temperature, (ii) reduced idle chiller capacity from higher demands, and (iii) the narrow charging window. The chillers' cooling capacity must be extraordinarily oversized for I-TES to be used in the high-demand season. This challenge can be alleviated with more efficient cooling technologies and buildings, and long-term energy storage technologies that could exploit large surplus PV generation in late spring prior to the high cooling season. BESS, on the other hand, is suited to meet the near year-round constant baseload.

The developed capacity sizing strategy can be broadly applied to buildings with different cooling technologies and under different climatic conditions. Furthermore, the strategy can also be applied to buildings with existing cooling technology for integration with other intermittent renewable energy resources. The strategy enables buildings to cost-effectively achieve a lower carbon footprint while taking into consideration the reliability of the system.

Limitations of the study include the moderately simplified models that may not fully capture all the complex behavior of multi-chillers systems. Additionally, the chosen performance curves for different chillers types may not fully represent the performances variations from various manufacturers. Future research could explore additional representative curves and include heating systems, though this may increase computational time

Appendix

The performances and costs of considered system components are decided based on current market offerings. Three chillers are selected from the EnergyPlus water-cooled chillers library to represent the typical performance of their compressor type. The data library contains chillers data with three distinct compressor types: centrifugal, centrifugal with a VSD, and screw compressor. The selected chillers are 365-tons Carrier 19XR with centrifugal compressor, 383-tons Carrier 19XR with VSD centrifugal compressor, and 340-tons Carrier 23XL with slide valve equipped screw compressor. To account for the improvement in cooling performance observed in chillers with larger capacities, the effective chiller COP is linearly adjusted with the capacity relative to the reference chiller COP by approximately 10^{-3} TR^{-1} per unit increase in capacity from nominal capacity.

Table 4 tabulates the characteristics and performance parameters used in the model. A 98% efficiency inverter is assumed for on-site PV. Generic BESS performance was assumed with charge and discharge efficiencies of 92%, which also account for inverter losses and a self-discharge efficiency of 99.9%.

Table 4: Characteristics parameters in the model

Item	Parameter	Symbol	Value
PV	Inverter Efficiency	η^I	98%
	Charge Efficiency	$\eta^{BESS,chs}$	92%
BESS	Discharge Efficiency	$\eta^{BESS,dis}$	92%
	Self-discharge Efficiency	$\eta^{BESS,sdis}$	99.9%
I-TES	Self-discharge Efficiency	$\eta^{I-TES,sdis}$	99.9%
Chiller	Improvement in COP per change in cooling capacity		10^{-3} TR^{-1}

The considered financial parameters are tabulated in Table 5. Installed fixed-tilt PV Capex was assumed to be on the lower ends at \$600/kW_{p,dc} and OpEx to be \$10/kW_{p,dc}/year. Small-scale 4-hour BESS was taken at the average market price of \$300/kWh. With access to cheap capital in Qatar, the system was financed at a 3.5% interest rate with 25 years of service life for I-TES, chillers, and PV and 10 years for BESS.

Table 5: Financial parameters in the model

Item	Unit	Expense	Symbol	Value
PV	Fixed-tilt	Capex	$c^{PV,C}$	\$600/kW _{p,dc}
		OpEx	$c^{PV,O}$	\$10/kW _{p,dc} /yr.
I-TES	Internal melt	Capex	c^{ITES}	\$23/kW _{th} (\$80/TR-hr)
BESS	4-hour Li-ion	Capex	c^{BESS}	\$300/kWh
Chiller	Centrifugal w/o VSD	Capex	c_1^{chl}	\$115/kW _{th} (\$400/TR)
	Centrifugal w/ VSD	Capex	c_2^{chl}	\$130/kW _{th} (\$450/TR)
	Screw w/o VSD	Capex	c_3^{chl}	\$100/kW _{th} (\$350/TR)
	Pumps w/o VSD	Capex	$c^{P,FS}$	\$150/kW
Auxiliary Equipment	Pumps w/ VSD	Capex	$c^{P,VSD}$	\$200/kW
	Cooling Tower	Capex	c^{twr}	\$57/kW _{th} (\$200/TR)
Misc.	Capital	Interest Rate	ir	3.5%
		Service Life	yr	25 years
		BESS Service Life	yrb	10 years

Similarly, based on current market offerings and published cost figures for WC CWS and I-TES. The cost of I-TES was \$80/TR-hr (\$14/kW_{th}). Centrifugal chillers were at \$400/TR with an additional \$50/TR for a VSD. Screw chillers cost less but are generally less efficient at \$350/TR. The cost for water pumps was \$150/kW and an additional \$50/kW for a VSD. Last, the cost of cooling towers was \$57/kW_{th} (\$200/TR) at the standard design 6°C water temperature differential; a larger temperature differential reduces the tower size and cost.

Acknowledgment

This research was sponsored by Qgrants through Qatar National Research Fund (QNRF) with a grant number QRLP10-G-1803028.

References

- [1] Intergovernmental Panel on Climate Change, Climate Change 2014: Mitigation of Climate Change, 2015. <https://doi.org/10.1017/cbo9781107415416>.
- [2] S. McCulloch, E. Masanet, J. Dulac, T. Abergel, S.D. Kira West, A.F. Pales, R.M. Uwe Remme, Luis Munera, A. Brown, T. Stanley, Energy Technology Perspectives 2017 - Catalysing Energy Technology Transformations, 2017. https://doi.org/10.1787/energy_tech-2017-en.
- [3] L.F. Cabeza, D. Urge-Vorsatz, M.A. McNeil, C. Barreneche, S. Serrano, Investigating greenhouse challenge from growing trends of electricity consumption through home appliances in buildings, Renewable and Sustainable Energy Reviews 36 (2014) 188–193. <https://doi.org/10.1016/j.rser.2014.04.053>.

- [4] L. Pérez-Lombard, J. Ortiz, C. Pout, A review on buildings energy consumption information, *Energy Build* 40 (2008) 394–398. <https://doi.org/10.1016/j.enbuild.2007.03.007>.
- [5] F. Saffouri, I.S. Bayram, M. Koc, Quantifying the Cost of Cooling in Qatar, (2018) 1–9. <https://doi.org/10.1109/ieeegcc.2017.8448269>.
- [6] I. Al-Aali, V. Modi, Decarbonizing the electricity sector in Qatar using PV combined with ice thermal and battery storage, *Energy Strategy Reviews* 44 (2022) 101014. <https://doi.org/10.1016/j.esr.2022.101014>.
- [7] M. Bohra, N. Shah, Optimising the role of solar PV in Qatar’s power sector, *Energy Reports* 6 (2020) 194–198. <https://doi.org/10.1016/j.egy.2019.11.062>.
- [8] N. Mohandes, A. Sanfilippo, M. Al Fakhri, Modeling residential adoption of solar energy in the Arabian Gulf Region, *Renew Energy* 131 (2019) 381–389. <https://doi.org/10.1016/j.renene.2018.07.048>.
- [9] H. Maammour, A. Hamidat, L. Loukarfi, M. Missoum, K. Abdeladim, T. Nacer, Performance investigation of grid-connected PV systems for family farms: Case study of North-West of Algeria, *Renewable and Sustainable Energy Reviews* 78 (2017) 1208–1220. <https://doi.org/10.1016/j.rser.2017.05.004>.
- [10] T.A. Deetjen, J.S. Vitter, A.S. Reimers, M.E. Webber, Optimal dispatch and equipment sizing of a residential central utility plant for improving rooftop solar integration, *Energy* 147 (2018) 1044–1059. <https://doi.org/10.1016/j.energy.2018.01.110>.
- [11] B. Mohandes, S. Acharya, S. Member, Optimal Design of an Islanded Microgrid With Load Shifting Mechanism Between Electrical, 35 (2020) 2642–2657.
- [12] Q. Zhu, Q. Li, B. Zhang, L. Wang, G. Li, R. Wang, Capacity optimization for electrical and thermal energy storage in multi-energy building energy system, *Energy Procedia* 158 (2019) 6425–6430. <https://doi.org/10.1016/j.egypro.2019.01.183>.
- [13] Z. Xu, X. Guan, Q.S. Jia, J. Wu, D. Wang, S. Chen, Performance analysis and comparison on energy storage devices for smart building energy management, *IEEE Trans Smart Grid* 3 (2012) 2136–2147. <https://doi.org/10.1109/TSG.2012.2218836>.
- [14] J. McQuiston, F., Parker, J., & Spitler, Heating, Ventilating and, Air Conditioning, Sixth, 2005.
- [15] I. Al-Aali, A. Narayanaswamy, V. Modi, A novel algorithm for optimal equipment scheduling and dispatch of chilled water systems with ice thermal storage, *Energy Build* 274 (2022) 112422. <https://doi.org/10.1016/j.enbuild.2022.112422>.
- [16] Y.C. Chang, J.K. Lin, M.H. Chuang, Optimal chiller loading by genetic algorithm for reducing energy consumption, *Energy Build* 37 (2005) 147–155. <https://doi.org/10.1016/j.enbuild.2004.06.002>.
- [17] W.S. Lee, Y.T. Chen, Y. Kao, Optimal chiller loading by differential evolution algorithm for reducing energy consumption, *Energy Build* 43 (2011) 599–604. <https://doi.org/10.1016/j.enbuild.2010.10.028>.
- [18] Y.C. Chang, A novel energy conservation method - Optimal chiller loading, *Electric Power Systems Research* 69 (2004) 221–226. <https://doi.org/10.1016/j.epsr.2003.10.012>.
- [19] B. Silveti, Application fundamentals of ice-based thermal storage, *ASHRAE J* 44 (2002) 30–35.
- [20] S. Hanson, M. Schwedler, B. Bakkum, *Chiller System Design and Control*, 2011.
- [21] *Understanding the Properties of Glycol Solutions Prevents Design Errors in Pumping and Piping Applications*, Milwaukee, 2001.

- [22] K.H. Drees, Modeling and Control of Area Constrained Ice Storage Systems, Purdue University, 1994.
- [23] Y. Chen, M. Guo, Z. Chen, Z. Chen, Y. Ji, Physical energy and data-driven models in building energy prediction: A review, *Energy Reports* 8 (2022) 2656–2671. <https://doi.org/10.1016/j.egy.2022.01.162>.
- [24] N. Fumo, P. Mago, R. Luck, Methodology to estimate building energy consumption using EnergyPlus Benchmark Models, *Energy Build* 42 (2010) 2331–2337. <https://doi.org/10.1016/j.enbuild.2010.07.027>.
- [25] M.T. Ke, C.H. Yeh, J.T. Jian, Analysis of building energy consumption parameters and energy savings measurement and verification by applying eQUEST software, *Energy Build* 61 (2013) 100–107. <https://doi.org/10.1016/j.enbuild.2013.02.012>.
- [26] M. Manfren, P. Ab, L. Tronchin, Data-driven building energy modelling – An analysis of the potential for generalisation through interpretable machine learning, *Renewable and Sustainable Energy Reviews* 167 (2022) 112686. <https://doi.org/10.1016/j.rser.2022.112686>.
- [27] Z. Wang, T. Hong, M.A. Piette, Building thermal load prediction through shallow machine learning and deep learning, *Appl Energy* 263 (2020) 114683. <https://doi.org/10.1016/j.apenergy.2020.114683>.
- [28] L. Duanmu, Z. Wang, Z.J. Zhai, X. Li, A simplified method to predict hourly building cooling load for urban energy planning, *Energy Build* 58 (2013) 281–291. <https://doi.org/10.1016/j.enbuild.2012.11.029>.
- [29] F. Johari, J. Munkhammar, F. Shadram, J. Widén, Evaluation of simplified building energy models for urban-scale energy analysis of buildings, *Build Environ* 211 (2022) 108684. <https://doi.org/10.1016/j.buildenv.2021.108684>.
- [30] B. Howard, L. Parshall, J. Thompson, S. Hammer, J. Dickinson, V. Modi, Spatial distribution of urban building energy consumption by end use, *Energy Build* 45 (2012) 141–151. <https://doi.org/10.1016/j.enbuild.2011.10.061>.
- [31] M. Krarti, F. Ali, A. Alaidroos, M. Houchati, Macro-economic benefit analysis of large scale building energy efficiency programs in Qatar, *International Journal of Sustainable Built Environment* 6 (2017) 597–609. <https://doi.org/10.1016/j.ijbsbe.2017.12.006>.
- [32] O. Alrawi, I.S. Bayram, M. Koc, High-resolution electricity load profiles of selected houses in Qatar, *Proceedings - 2018 IEEE 12th International Conference on Compatibility, Power Electronics and Power Engineering, CPE-POWERENG 2018* (2018) 1–6. <https://doi.org/10.1109/CPE.2018.8372569>.
- [33] O. Alrawi, I.S. Bayram, S.G. Al-Ghamdi, M. Koc, High-resolution household load profiling and evaluation of rooftop PV systems in selected houses in Qatar, *Energies (Basel)* 12 (2019). <https://doi.org/10.3390/en12203876>.
- [34] Kahramaa, Tariff, Kahramaa (2019). <https://www.km.com.qa/CustomerService/Pages/Tariff.aspx> (accessed October 3, 2019).